energies

MDPI

Review

Energy Dissipation and Efficiency Challenges of Cryogenic Sloshing in Aerospace Propellant Tanks: A Systematic Review

Alih John Eko [1,2,*], Xuesen Zeng [1], Mazahar Peerzada [1], Tristan Shelley [1], Jayantha Epaarachchi [1,2] and Cam Minh Tri Tien [1]

[1] Centre for Future Materials & Institute of Advanced Engineering and Space Sciences, University of Southern Queensland, Toowoomba, QLD 4350, Australia
[2] School of Engineering, Faculty of Health, Engineering and Sciences, University of Southern Queensland, Toowoomba, QLD 4350, Australia
* Correspondence: john.eko@unisq.edu.au

Abstract

Cryogenic propellant sloshing presents significant challenges in aerospace systems, inducing vehicle instability, structural fatigue, energy losses, and complex thermal management issues. This review synthesizes experimental, analytical, and numerical advances with an emphasis on energy dissipation and conversion efficiency in propellant storage and transfer. Recent developments in computational fluid dynamics (CFD) and AI-driven digital-twin frameworks are critically examined alongside the influences of tank materials, baffle configurations, and operating conditions. Unlike conventional fluids, cryogenic propellants in microgravity and within composite overwrapped pressure vessels (COPVs) exhibit unique thermodynamic and dynamic couplings that remain only partially characterized. Prior reviews have typically treated these factors in isolation; here, they are unified through an integrated perspective linking cryogenic thermo-physics, reduced-gravity hydrodynamics, and fluid–structure interactions. Persistent research limitations are identified in the areas of data availability, model validation, and thermo-mechanical coupling fidelity, underscoring the need for scalable multi-physics approaches. This review's contribution lies in consolidating these interdisciplinary domains while outlining a roadmap toward experimentally validated, AI-augmented digital-twin architectures for improved energy efficiency, reliability, and propellant stability in next-generation aerospace missions.

Keywords: cryogenic sloshing; energy dissipation; conversion efficiency; propellant tanks; aerospace vehicles; prediction methods

check for updates

Academic Editor: Magdalena Piasecka

Received: 23 September 2025
Revised: 5 October 2025
Accepted: 10 October 2025
Published: 11 October 2025

Citation: Eko, A.J.; Zeng, X.; Peerzada, M.; Shelley, T.; Epaarachchi, J.; Tien, C.M.T. Energy Dissipation and Efficiency Challenges of Cryogenic Sloshing in Aerospace Propellant Tanks: A Systematic Review. *Energies* **2025**, *18*, 5362. https://doi.org/10.3390/en18205362

Copyright: © 2025 by the authors. Licensee MDPI, Basel, Switzerland. This article is an open access article distributed under the terms and conditions of the Creative Commons Attribution (CC BY) license (https://creativecommons.org/licenses/by/4.0/).

1. Introduction

Cryogenic propellants are fuels and oxidizers stored at extremely low temperatures to maintain their liquid phase, thereby enabling high-performance rocket propulsion. They are indispensable for space exploration because of their high specific impulse, which directly enhances the efficiency of launch and in-space transportation systems. In practice, the primary cryogenic propellants are liquid hydrogen (LH_2, boiling point 20.27 K/−252.88 °C/−423.18 °F), liquid oxygen (LOX, 90.19 K/−182.96 °C/−297.33 °F), and liquid methane (LCH_4, 111.66 K/−161.49 °C/−258.68 °F), which serve as the main propulsive fuels and oxidizers. Other cryogenic fluids, such as liquid nitrogen (LN_2, 77.36 K/−195.79 °C/−320.42 °F), liquid argon (LAr, 87.30 K/−185.85 °C/−302.53 °F), and liquid fluorine (LF_2, 85.03 K/−188.12 °C/−306.62 °F), are not generally employed as

power propellants but have critical roles in aerospace systems. For instance, LN_2 is widely used as a simulant for cryogenic propellant sloshing studies, as a pressurant and coolant in ground and flight systems, and as a working 6 fluid in cold-gas thrusters for satellite attitude control. Additionally, slush hydrogen (SLH_2) a solid–liquid mixture of hydrogen maintained below 20.27 K (−252.88 °C/−423.18 °F) has been developed to increase storage density and efficiency [1–4].

Cryogenic propellants have long enabled high-performance rocketry, but the real bottleneck today is not just storing very cold fluids; it is minimizing the relentless energy losses that erode mission margins. Figure 1 shows a representative cryogenic tank, where every watt of parasitic heat leak (through supports, penetrations, and imperfect MLI), every vented gram from boil-off control, and every transient during chill-down, pressurization, or settling translates directly into lost propulsive efficiency. In microgravity, additional penalties arise stratification and geysering complicate autogenous pressurization, sloshing and vapour ingestion force conservative throttle windows, and propellant management devices incur pressure drops that must be overcome each form of dissipated useful energy [5,6].

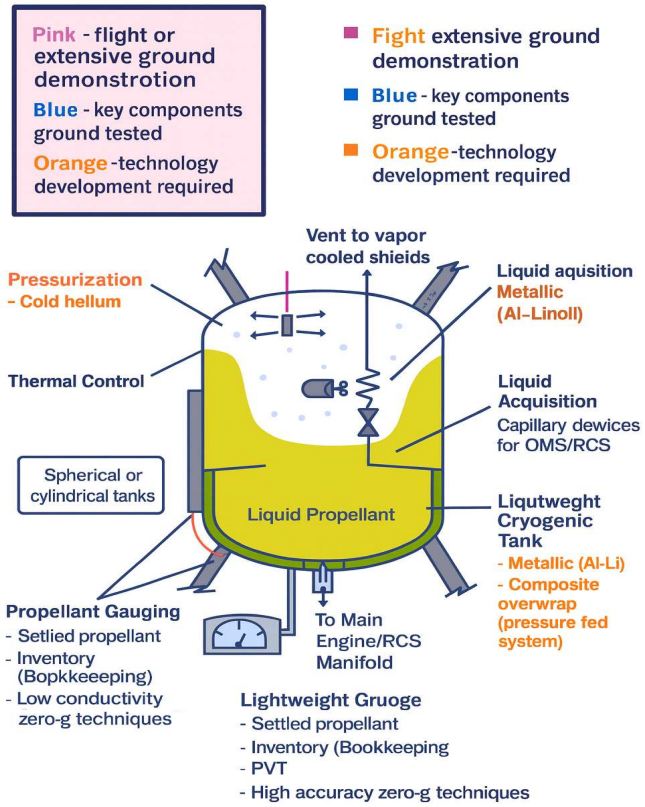

Figure 1. The schematics of a cryogenic Storage Tank [7].

Historically, early Mercury-era drop-tower tests and the Centaur/S-IV operational stages proved cryogenic propulsion's promise while revealing its inefficiencies over time: extended loiter meant mounting boil-off, venting losses, and thermal cycling of tanks. Since then, Cryogenic Fluid Management (CFM) research has increasingly targeted the full dissipation path from external heat leaks to internal mixing and vent control. Programs such as CONE, CFME, and the proposed COLD-Sat reframed the problem around quantifying and closing energy budgets in reduced gravity. Building on that, the CPST campaign focuses on system-level demonstrations: advanced thermal control to suppress boil-off, low-loss transfer and chill-down to cut start-up waste, and integrated operations that keep vapour generation and venting within tight bounds over mission timelines.

Densification is a powerful lever in this efficiency picture. Subcooling LH_2 and LOX to boost density (≈8% and ≈10%, respectively) improves tankage fraction and can drive vehicle gross-mass reductions on the order of tens of percent. But that gain is only net-positive if the refrigeration work, ground-side handling penalties, and on-orbit heat-soak margins are managed so the saved structural and boil-off energy outweigh the extra cooling cost. Modern efforts including renewed interest in subcooled and slush propellants therefore treat densification not as a static property change, but as a system optimization: reduce boil-off, preserve pump NPSH margins, shorten chill-down, and limit venting, all while keeping the refrigeration energy and added complexity within the overall mission energy budget.

Research on cryogenic fluid management in microgravity has increasingly focused on identifying and minimizing sources of energy dissipation, since every inefficiency whether through boil-off, venting, pressure drop, or thermal cycling directly reduces mission performance. Technologies such as Propellant Management Devices (PMD), Zero Boil-Off (ZBO) tanks, Vapour Cooling Systems (VCS), Thermodynamic Vent Systems (TVS), Propellant Transfer and Chill-Down (PTCD/TO), and Heterogeneous/Autogenous Pressurization (HP/AP) are all ultimately aimed at mitigating these dissipative pathways. For example, Ming He et al. [8] optimized the design of a cryo-compressed hydrogen refuelling station by developing a heat transfer model to evaluate dynamic temperature evolution during precooling. Their work compared different inlet-diameter strategies and showed that the constant mass flow approach not only reduced hydrogen losses and boil-off, but also minimized thermal stresses on the tank, effectively eliminating the need for auxiliary heating. This illustrates how proper thermal and flow control directly translates to improved energy efficiency and reduced dissipation.

Among the most prominent energy-related inefficiencies is sloshing, the oscillatory motion of propellant within partially filled tanks. In everyday terms, it resembles coffee sloshing in a cup, but in aerospace it generates unplanned energy transfers that couple into vehicle dynamics, degrading stability and wasting control authority. NASA's early investigations in the 1960s revealed how sloshing not only dissipates energy internally through turbulence and wave breaking but also forces external corrective actions that consume additional propulsive energy. These findings shaped the design of Centaur and Saturn stages, where engineers had to account for venting, pressurization, and roll control losses tied to slosh-driven disturbances.

Energy dissipation from sloshing is not unique to spacecraft. In ships, it reduces ballast efficiency; in cars and trains, it alters handling and braking forces. But in launch vehicles where liquid propellants dominate the gross mass fraction sloshing losses are magnified by the extreme acceleration environment. Every uncontrolled oscillation can force actuators and control systems to counteract wasted dynamic loads, consuming propellant and potentially inducing resonant oscillations that amplify dissipation further. For instance, early Saturn I missions demonstrated how roll instabilities were linked to sloshing resonance, forcing additional energy expenditure in stabilization.

The degree of dissipation depends strongly on tank configuration. Large-diameter cylindrical tanks tend to have lower natural frequencies, making them more prone to resonance with structural or control-system modes, thus raising dissipation risks. Subdivided tanks or internal baffles can shift sloshing frequencies upward, but this introduces additional viscous losses and pressure drops, creating new energy pathways that must be balanced against control savings. As shown in Figure 2, vehicle designers must therefore trade between slosh suppression (reducing dynamic losses) and structural efficiency (avoiding overbuilt, heavy solutions). Ultimately, sloshing is not just a fluid-mechanics curiosity it is a core energy challenge. Unchecked, it dissipates energy both internally (through mixing

and turbulence) and externally (through unnecessary control work), reducing the overall efficiency of cryogenic propulsion systems [9].

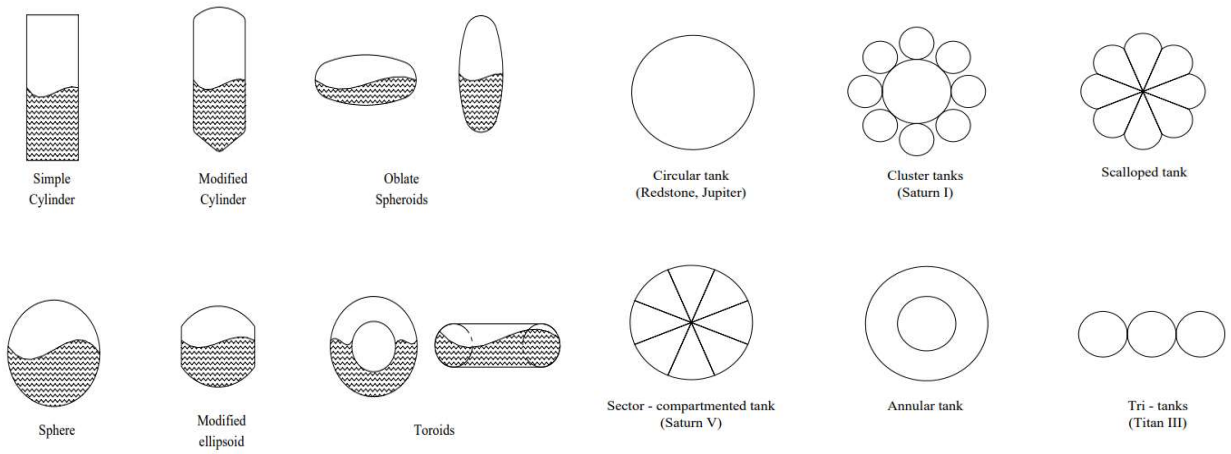

Figure 2. An illustration of the tank configuration for the space vehicle on the left and the launch vehicle on the right [9].

Sloshing manifests in multiple modes, each representing not just a stability issue but a pathway for energy dissipation that reduces overall propulsive efficiency. Lateral sloshing, driven by translational or pitching motions, dissipates energy into transverse oscillations that disturb trajectory control and force additional corrective thrusting. Vertical sloshing, induced by accelerations normal to the liquid surface, destabilizes propellant distribution and introduces interruptions in delivery, requiring pump or pressurization systems to expend extra energy to compensate. Swirl sloshing, triggered by vehicle roll or yaw, generates rotational flow structures that increase mixing losses and pressure drops, ultimately raising the energy cost of stable engine feed. At the extreme, vortex formation as illustrated in Figure 3 and spray events represent direct propellant loss both wasted mass and wasted energy embedded in producing, storing, and cooling that propellant in the first place. In microgravity, where surface tension dominates, sloshing becomes highly unpredictable, creating irregular distributions that compromise the efficiency of transfer operations and orbital manoeuvres.

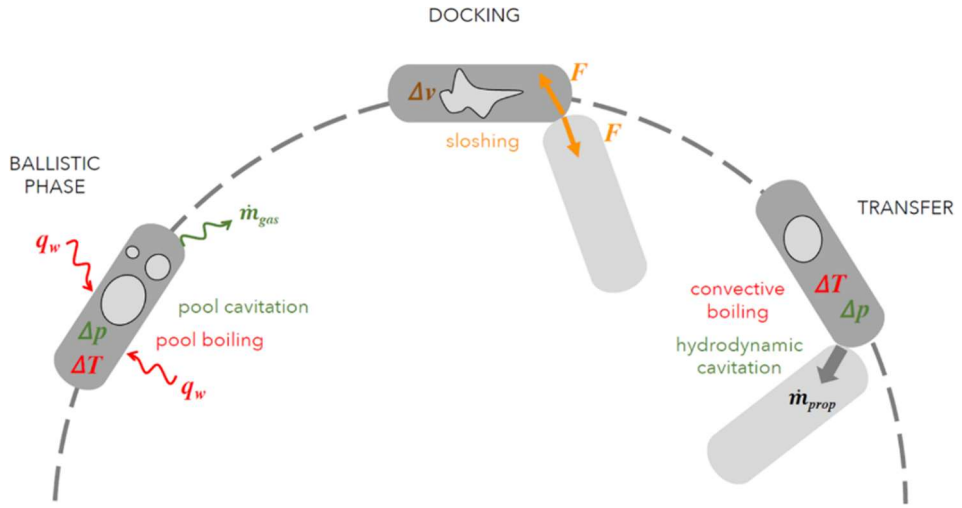

Figure 3. The three operations represented are ballistic phase, docking and transfer. For each phase, the most typical physical phenomena occurring is represented: in green the phenomena dominated by a variation in pressure, in red those dominated by a variation in temperature and in yellow those dominated by a variation of velocity [10].

The absence of hydrostatic pressure in microgravity exacerbates these losses. Without gravity-driven stratification, cryogenic fluids can assume unstable or asymmetric configurations that shift the vehicle's centre of mass, forcing continuous control corrections and wasting valuable propulsive energy. Uncontrolled sloshing also produces dynamic pressure fluctuations, transferring cyclic loads into tank walls and baffles. Over time, this leads to structural fatigue, a hidden form of energy dissipation was absorbed oscillatory energy gradually weakens materials. Sensor systems such as capacitance or thermal probes experience noise from sloshing, reducing the accuracy of gauging and often requiring redundant sensing or computational filtering, both of which add system-level energy cost. Interaction with internal structures (baffles, diaphragms) converts ordered oscillations into localized turbulence, raising heat transfer coefficients and increasing boil-off rates. In hydrogen systems, where density is low and volatility high, these localized disturbances translate into particularly high efficiency penalties.

Mitigating these losses requires accurate modelling and careful frequency management. If sloshing frequencies overlap with vehicle or control-system natural modes, resonance can amplify dissipation dramatically. Conversely, well-designed baffles or tank subdivisions can redirect slosh energy into higher-frequency modes where control systems can damp them more efficiently. Effective slosh mitigation is therefore not just a stability requirement it is an energy optimization strategy, ensuring that stored cryogens retain their useful enthalpy, control systems expend less corrective work, and mission energy budgets remain within acceptable bounds. This is especially vital for long-duration or reusable hydrogen-fueled vehicles, where even small rates of dissipation, if unchecked, accumulate into mission-threatening inefficiencies.

One of the most significant case studies highlighting the importance of understanding sloshing behaviour occurred during the Boeing Delta IV second-stage launch. In a particular mission, an independent review team from Analex Corporation identified discrepancies in the predicted behaviour of the second-stage cryogenic propellants, which differed significantly from the simulations conducted by Boeing and the Aerospace Corporation. Concerned about the potential risks, Boeing recommended delaying the launch until the inconsistencies were resolved. A collaborative investigation involving Boeing, the U.S. Air Force, the Aerospace Corporation, Flow Sciences, and Analex ultimately revealed that the liquid hydrogen (LH_2) in the second-stage tank was not constrained to the aft end during the coast phase, posing a serious mission risk. The unexpected presence of propellant in the forward dome of the tank venting could have resulted in propellant ingestion into the vent/relief system, leading to a thrust imbalance. To mitigate this issue, the team implemented a pulse-settling approach for propellant management, demonstrating the critical need for accurate sloshing behaviour predictions in spaceflight operations [11].

2. Basic Equations of Sloshing and Heat Transfer in Cryogenic Pressure Vessel

Understanding the coupled dynamics of sloshing and heat transfer in cryogenic pressure vessels is essential for predicting vehicle stability, structural integrity, and long-term propellant retention. Sloshing defines the natural frequencies and hydrodynamic forces induced when the liquid mass oscillates under external excitations, directly influencing guidance and control margins as well as structural fatigue. Heat transfer, in parallel, governs the rate of energy ingress through conduction, convection, and radiation, ultimately driving liquid vaporization and boil-off that degrade performance and reduce mission endurance. Both phenomena are tightly linked: vigorous sloshing enhances internal convection, accelerates wall-to-fluid heat exchange, and can amplify boil-off in low-gravity environments. To capture these effects, simplified analytical models provide first-order es-

timates of slosh frequencies, forces, and pressure rise, while classical heat-transfer relations quantify thermal leakage and boil-off rates. Although these formulations rely on idealized assumptions rigid walls, small-amplitude motion, gray/diffuse surfaces they remain indispensable for preliminary design, system sizing, and control-law development. More advanced CFD, SPH, and FSI models can resolve nonlinearities and microgravity-specific behaviours, but the analytical framework presented here establishes the baseline equations used to characterize sloshing and heat transfer in cryogenic tanks [12], and to highlight the trade-offs that drive insulation design, baffle placement, and thermal control strategies.

To calculate the natural frequency of a cylindrical tank, the equations are expressed as follows

$$\omega_m^2 = \frac{\xi_m g}{r \tanh\left(\frac{\xi_m h}{r}\right)} \tag{1}$$

$$f_m = \frac{\omega_m}{2\pi} \tag{2}$$

where ω_m means the angular frequency cylindrical tank (rads^{-1}), r is the tank radius, g is the gravitational acceleration, h is the liquid height, and ξ_m denotes the root of the eigenvalue equation. For the natural frequency of a spherical Tank the expressions used are:

$$\omega_n = \frac{1}{2\pi}\sqrt{\frac{\lambda g}{R}} \tag{3}$$

where ω_n is the natural angular frequency (spherical tank) g is the gravitational acceleration, R tank radius, λ the empirical constant based on liquid height and tank radius.

The natural frequency for both planar and non-planar motion can be estimated using these equations:

$$\left(\frac{\omega_0}{\omega_n}\right)^2 = K_1 + K_2\left(\frac{X_0}{2R}\right)^{\frac{2}{3}} \tag{4}$$

ω_0 is the excitation frequency, X_0 The excitation amplitude $K_{1,2}$ are the empirical constants [13–15].

Equations (1) and (2) (natural slosh frequency in cylindrical tanks), consider small-amplitude eigenmodes in a right circular cylinder at a specified fill height under a given gravity level, assuming inviscid potential flow, rigid walls, and linear free-surface motion; it matters because it flags resonance with vehicle/attitude-control modes and informs baffle spacing and controller detuning; limitations: large amplitudes, internal hardware/baffles, and micro-g capillary effects shift frequencies and add damping beyond linear theory; for Equation (3) (natural slosh frequency in spherical tanks), consider the first-mode response with a fill-dependent parameter λ under linear potential-flow assumptions and rigid boundaries; it matters because spherical LH_2/LOX tanks are common and the mode frequency bounds loads and control bandwidth; limitations: contact-line hysteresis and capillary dominance in low-g invalidate linear predictions and increase fill-ratio sensitivity; and for Equation (4) (nonlinear/empirical amplitude–frequency correction), consider frequency softening/stiffening under finite excitation amplitude X_0 relative to geometry R with coefficients K_1, K_2 fitted over a tested range; it matters because it captures operational resonance shifts during large manoeuvres not seen in linear spectra; limitations: coefficients are not universal and must be re-identified for tank geometry, fill level, and the presence of baffles/internals.

Sloshing Forces and Moments. Under external excitation, the fluid exerts pressure and viscous shear on the wetted walls. The resultant hydrodynamic wall force and moment transmitted to the structure are obtained by integrating these stresses over all wall faces:

$$\mathrm{F_s} = \sum_{\mathrm{i}\in \mathrm{A_{wall}}} (\mathrm{F_{P,i}} + \mathrm{F_{v,i}}) \tag{5}$$

$$F_s^{(\hat{a})} = \hat{a} \cdot F_s \left(\text{component along } \hat{a}\right) \tag{6}$$

where $\mathrm{F_{P,i}}, \mathrm{F_{v,i}}$ respectively, the pressure and viscous (shear) contributions integrated over wall face i, r_i and is the position vector from a chosen reference point O to the force application point (e.g., face centroid). When a scalar component along $\hat{a}$ unit direction is needed (e.g., body × load), use:

$$M_s = \sum_i r_i \times (F_{P,i} + F_{v,i}) \tag{7}$$

The scenario is hydrodynamic moment from wall stresses about a chosen origin via r × F the assumptions are the same as for force integration with a well-defined reference point; it matters because moments' drive pointing errors and control saturation; limitations: sensitive to free-surface breakup resolution and ignores structural flexibility unless co-simulated.

Heat transfer in cryogenic pressure vessels occurs through three primary mechanisms: conduction, convection, and radiation. The extent of heat ingress is influenced by the thermal properties of the vessel materials, the effectiveness of insulation, and the surrounding environmental conditions. In cryogenic environments, conventional thermal behaviour is altered; properties such as thermal conductivity, specific heat capacity, and boundary layer characteristics are significantly affected. Even minimal heat leakage from the ambient environment can lead to rapid vaporization of the stored cryogenic liquid, which may compromise operational safety, efficiency, and mission duration, especially in aerospace applications. The scenario is partitioning external heat leaks (radiation/solid/gas paths) minus wall heat soak to obtain heat absorbed by the cryogen over Δt the assumptions are quasi-steady boundary fluxes and lumped wall thermal storage; it matters because it links insulation and structure to actual boil-off/pressurization; limitations: spatial transients and strong wall–fluid coupling are reduced to lumped terms, so early-time behaviour may be misrepresented.

The amount of heat absorbed by the contained hydrogen corresponds to the net heat transferred to the vessel through radiation, solid conduction, gaseous conduction, and natural convection, minus the amount of heat stored within the vessel's structure. Natural convection arises both externally between the outer wall of the storage tank and the surrounding ambient environment and internally, between the inner wall and the vapour/liquid phases, as well as between the vapour and liquid phases.

$$\Delta \mathrm{Q_{abs}} = \left(\mathrm{Q_r} + \mathrm{Q_{sc}} + \mathrm{Q_{gc}}\right)\Delta \mathrm{t} - \Delta \mathrm{Q_s}\Big) \tag{8}$$

where is Q_r is the heat transfer by radiation, Q_{sc} the heat transfer by solid conduction. Q_{gc} the heat transfer by gaseous conduction, ΔQ_s heat stored in the vessel itself, ΔQ_{abs} net heat absorbed by the cryogenic hydrogen.

Radiative heat transfer between concentric spherical surfaces is influenced by surface temperatures, emissivities, and geometric parameters such as sphere diameters. It contributes significantly to total heat ingress in cryogenic storage systems can be given as:

$$\frac{\mathrm{Q_r}}{\mathrm{A_s}} = \frac{\sigma\left(\mathrm{T_h^4} - \mathrm{T_s^4}\right)}{\frac{1}{\epsilon_s} + \frac{\mathrm{A_s}}{\mathrm{A_h}}\left(\frac{1}{\epsilon_h} - 1\right)} \tag{9}$$

Q_r is the radiative heat transfer (W), A_s the surface area of the inner (smaller) sphere (m^2), A_h the surface area of the outer(larger) sphere (m^2), T_h , T_s the temperatures of the outer and inner surfaces (K), $\in_h$, $\in_s$ the emissivites of the outer and inner surface, σ The Stefan–Boltzmann constant ($5.67{\cdot}10^{-8}\frac{W}{m^2}{\cdot}k^4$) based on the assumptions that both surfaces are gray, resulting in negligible calculation errors. It also assumes diffuse reflections, rather than specular ones, and that both surfaces have uniform temperatures. Given the use of flat black paint on the surfaces, diffuse reflections are highly likely. In calculating the radiant heat transfer, the temperature of each heater hemisphere was treated individually. The scenario is vacuum radiation between inner and outer shields/shells; the assumptions are gray, diffuse, isothermal surfaces with known areas/view factors; it matters because radiation sets the floor heat leak in well-evacuated systems and informs MLI/VCS design; limitations: real MLI is multilayered and non-gray with edge/leak paths not captured by the simple enclosure formula.

In cryogenic pressure vessels, solid conduction is a key mechanism of heat transfer, allowing heat to flow through the vessel's walls or insulation layers. As heat moves from the hotter to the cooler side, particles within the material, such as atoms or molecules, vibrate or move, transferring their energy to neighbouring particles. The rate of heat transfer via conduction depends on the material's thermal conductivity and the temperature gradient across it. This process can influence the stability and efficiency of the stored cryogenic fluid by affecting its temperature and phase state. It can be expressed by:

$$\frac{Q_{sc}}{A_{sc}} = \frac{k}{l}\Delta T \tag{10}$$

Q_s is the heat transferred by conduction, A_{sc} is the cross-sectional area through which heat is transferred, while k the thermal conductivity of the material, indicating how easily heat can flow through the material, l is the thickness of the material through which heat is transferred. ΔT is the temperature difference across the material.

Gaseous conduction is the transfer of heat through a gas due to a temperature gradient. In cryogenic systems, it occurs when a temperature difference exists between the gas inside the vessel and its surroundings. Heat flows from the warmer region to the cooler one, with gas molecules transferring energy through collisions. The rate of heat transfer depends on factors like the temperature difference, the gas' thermal conductivity, and the space geometry. In cryogenic pressure vessels, gaseous conduction plays a crucial role in thermal management, influencing the cryogenic fluid's stability and system efficiency. The rate of heat transfer is described by a simplified version of Fourier's Law for gases. The scenario is heat transfer across an annulus when residual gas remains in insulation gaps; the assumptions are correlation parameters valid for the gas species, pressure, and Knudsen regime; it matters because vacuum quality drift can sharply raise heat leak and boil-off; limitations: continuum correlations fail in free-molecular flow, requiring rarefied-gas models. Expressed by:

$$\frac{Q_{gc}}{A_s} = K(\frac{r+1}{r-1})\left[\frac{a_s a_h}{a_h + a_s(1-a_h)\frac{A_s}{A_h}}\right]\left(\frac{P_G}{\sqrt{MT_G}}\right)(T_h - T_s) \tag{11}$$

The heat absorbed by the container wall is determined by the specific heat capacity of the material, the weight (or mass) of the container, and the temperature change. This relationship can be expressed by the equation:

$$\Delta Q_s = WC_p \cdot \Delta T_s \quad (12)$$

where ΔQ_s is the heat absorbed or released by the system (in the container wall), W is the weight or mass of the container, C_p is the specific heat capacity at constant pressure (a material property), ΔT_s the change in the temperature of the system container wall The scenario is energy absorbed by the tank structure as its temperature changes; the assumptions are lumped mass and specific heat with a representative wall temperature change; it matters because structural inertia delays pressurization and changes cryocooler/TVS duty cycles; limitations: gradients, coatings, and multilayer stacks violate the lumped assumption.

This equation is used to calculate the amount of heat absorbed or released by the walls of a cryogenic pressure vessel as its temperature changes. The equation considers the vessel's mass (or weight), the specific heat capacity of the material, and the temperature change. In cryogenic pressure vessels, the container's wall can absorb heat from the environment or release heat into the stored cryogenic fluid, depending on the temperature differential. The rate of heat absorption or release directly influences the thermal management of the vessel, potentially affecting the stability of the cryogenic fluid and the vessel's overall performance. Understanding and calculating this heat transfer is crucial for ensuring the cryogenic liquid remains within its desired temperature range and for maintaining the safety and efficiency of the system.

The phenomenon that occurs in cryogenic pressure vessels, known as boil-off, involves the evaporation of a portion of the cryogenic liquid due to heat ingress from the external environment. As heat from external sources gradually enters the vessel, it raises the temperature of the cryogenic liquid, causing it to reach its boiling point and transition from liquid to gas. This process is inevitable to some extent, even with well-insulated vessels, though the rate of boil-off can vary depending on the insulation quality, heat transfer, and the duration of exposure to external heat sources.

In cryogenic pressure vessels, managing boil-off is essential for maintaining the stability and efficiency of the stored liquid. Excessive boil-off can lead to a reduction in the amount of stored cryogenic fluid, affecting the pressure inside the vessel and potentially impacting the performance of the system. Understanding and controlling this phenomenon is crucial in various applications, such as space exploration and liquid hydrogen storage, to ensure safety, reliability, and optimal performance over extended periods. Which can be expressed by:

$$P_{bo} = \frac{(\text{Boiloffrate}) \cdot (\text{time})}{h_v V \rho_{sl}} \cdot 100 \text{ percent} \quad (13)$$

where P_{bo} The percentage of boil off, boil off rate is the rate at which the cryogenic liquid evaporates, time is the duration the boil off occurs, while h_v is the latent heat of vaporization of the cryogenic liquid. V is the volume of cryogenic liquid in the vessel, ρ_{sl} is the density of the cryogenic liquid at an initial stage. The scenario is converting a boil-off mass-rate over time into a percentage of stored liquid using latent heat and initial inventory; the assumptions are constant latent heat, volume, and density over the interval; it matters because it provides a mission-level loss metric and vent sizing input; limitations ignore transient stratification, time-varying properties, and interfacial kinetics.

The heat input to the contained mass of hydrogen, both liquid and vapour, in a cryogenic pressure vessel can indeed be calculated using the heat-transfer equations discussed earlier. With this heat input and knowledge of the mass of hydrogen, the pressure inside

the vessel can be determined for a constant volume system, assuming the contents are in thermal equilibrium.

The equation governing this process is derived from the first law of thermodynamics, which is based on the relationship between heat, work, and internal energy. The enthalpy definition also plays a role, as it relates the internal energy to the pressure and volume of the system.

For a constant volume process, the heat input (Q) leads to changes in both the internal energy and the enthalpy of the hydrogen. The relationship can be written as:

$$\mathrm{Q} = \Delta\mathrm{H} - \mathrm{v}\Delta\mathrm{P} \tag{14}$$

where ΔH is the enthalpy change in the system. Enthalpy is a thermodynamic property that reflects both the internal energy and the pressure-volume work of a system, while v is the specific volume of the fluid, which is the volume occupied by a unit mass of the substance. In the case of hydrogen, the specific volume depends on whether it is in the liquid or vapour phase, ΔP the change in pressure of the system. The scenario is relating net heat input to pressure rise in a sealed tank at fixed volume; the assumptions are near-equilibrium bulk phases and an effective specific volume; it matters because it gives a first-order prediction of ullage pressure growth for safety and control logic; limitations: two-temperature nonequilibrium, dissolved gases, and phase-change dynamics can cause significant deviations.

In practice, when heat is transferred to the system (through conduction, radiation, etc.), it increases the enthalpy of the hydrogen, which causes part of the liquid to vaporize and subsequently increases the pressure. The resulting pressure change (ΔP) is linked to the specific volume of the hydrogen, contributing to the overall heat balance in the system [16].

3. Sloshing in Microgravity Conditions

Sloshing, the oscillatory motion of a liquid free surface under external excitation, poses a significant challenge in cryogenic pressure vessel design, particularly in microgravity. Reduced gravity alters fluid behaviour, influencing liquid distribution, heat transfer, and system stability. These effects are especially pronounced in partially filled tanks, where slosh-driven oscillations lead to pressure fluctuations, stratification, and shifts in liquid positioning, all of which compromise the reliability of propellant storage and transfer. Numerical analyses show that sloshing is highly sensitive to both gravity level and fill fraction. Ji-Cheng Li et al. [17] found that in capsule-shaped tanks under low to microgravity, damping behaviour varies with fill level, ranging from underdamped at very low or high levels to nearly critically damped at intermediate levels. Their results also revealed that residual gravity and fill ratio strongly influence contact line stability and oscillation frequency. These findings highlight the need for adaptive damping solutions, with composite baffles capable of tailored stiffness and energy dissipation offering advantages over traditional aluminum designs.

Experimental and numerical evidence further emphasize the role of excitation frequency in determining slosh severity. Chaoran Hou et al. [18] investigated longitudinal excitation of liquid hydrogen and observed that low-frequency, large-amplitude disturbances promoted relatively stable free-surface behaviour, whereas high-frequency excitation caused pronounced gas–liquid interface deformation, jetting phenomena, and measurable propellant mass loss. Traditional baffles provided adequate mitigation at low frequencies but were ineffective at high-frequency excitation, demonstrating the limitations of conventional designs. These findings strengthen the case for composite baffles, which combine reduced mass with the potential for tailored damping and superior dynamic performance.

In addition to dynamic effects, thermal and phase-change phenomena critically influence cryogenic propellant management under microgravity conditions. Studies by Yaobin Jiang et al. [19], Jiaojiao Wang et al. [20], Jason Hartwig et al. [21], and Zhan Liu et al. [22] collectively revealed that in reduced-gravity environments, gravity levels, thermal gradients, fill ratios, and material interactions govern evaporation, bubble dynamics, and stratification in cryogenic tanks. As gravitational acceleration diminishes, surface tension and capillary forces become the primary drivers of liquid configuration and interface stability, dictating how the fluid adheres to tank walls and responds to perturbations. The overall fluid–structure interaction behaviour of the tank, as demonstrated by Weizhen Kong and Qiang Tian [23], is also highly sensitive to small variations in the effective gravitational field such as those induced by spacecraft manoeuvres, attitude changes, or transient accelerations that modify the inertial forces acting on the liquid. These findings emphasize the importance of integrated design strategies for microgravity operations, in which baffle materials with low thermal conductivity such as composites can simultaneously enhance capillary containment, thermal control, and slosh damping performance.

Finally, direct slosh mitigation devices such as slat screens have been explored as seen in Figure 4. Sobia Nadeem et al. reported promising, though variable, performance of such devices under certain operating conditions [24]. The partial effectiveness of these solutions suggests that more robust, broadly applicable baffle concepts are required. Within this context, advanced composite baffles emerge as highly promising, offering a pathway toward lightweight, thermally efficient, and dynamically robust designs for cryogenic propellant storage in space applications.

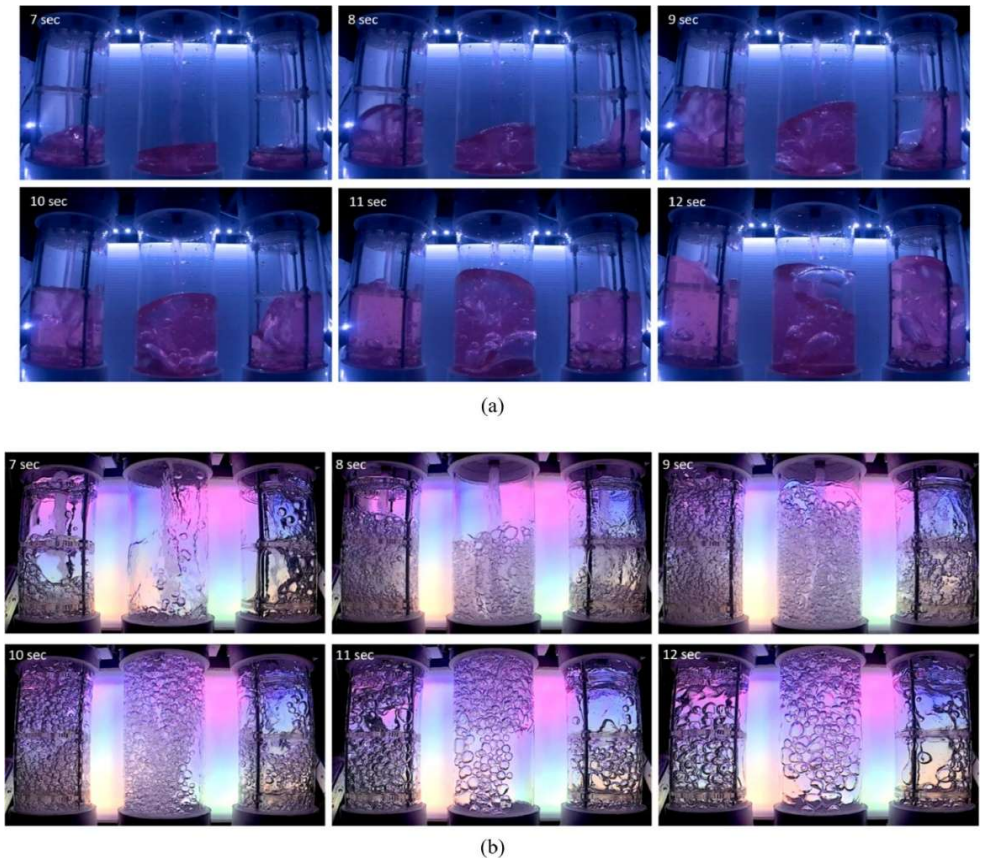

Figure 4. Footage of fluids under microgravity conditions during experiments using (**a**) Water and (**b**) FC-72, with a 75% fill rate in both cases. Each image captures stills of the fluid 7 to 12 s into the parabola. From left to right, the test chambers in each image contain the perforated slat screen, no slat screen, and the single-entry slat screen, respectively [24].

Romero-Calvo et al. [25] examined the sloshing dynamics of magnetic liquids in microgravity, addressing an important challenge for spacecraft propulsion and attitude control. Their work was carried out as part of the UNOOSA DropTES StELIUM project, which aimed to investigate lateral sloshing of ferrofluid solutions in inhomogeneous magnetic fields under microgravity conditions. The campaign, conducted in November 2019 at ZARM's Bremen drop tower, employed a carefully designed experimental platform integrating subsystems for actuation, detection, magnetic control, and structural stability, ensuring robust data collection.

To guarantee reliability, multiple redundant diagnostic systems including SDSs, GDS, and lateral cameras were deployed. This redundancy proved essential when two of the four experimental drops experienced partial subsystem failures due to high gravity accelerations. Despite these issues, the integrity of the scientific results was preserved. Free-surface deformation during sloshing was captured using a laser line technique, which enabled accurate surface reconstruction. Minor ripples caused by surface irregularities were observed but did not significantly affect the modal analysis.

Spectral analysis using Fast Fourier Transform (FFT) further revealed mode-dependent responses. Central measurements detected only the axisymmetric sloshing mode, whereas lateral sensors captured both the fundamental and second lateral modes. Notably, the largest amplitudes occurred at intermediate radial positions, while the tank wall exhibited mixed characteristics between free-edge and fixed-edge boundary conditions.

These results not only validated magnetic sloshing models but also contributed to a deeper understanding of ferrofluid behaviour in reduced gravity. The findings hold direct implications for the development of advanced magnetic liquid management strategies, which may enhance propellant handling and improve spacecraft stability and control in future missions.

Dalmon et al. [26] extended the understanding of sloshing under microgravity by combining experimental data from the FLUIDICS experiment aboard the International Space Station (ISS) with Direct Numerical Simulations (DNS) using the in-house DIVA solver. The study focused on spherical tanks rotated about a fixed axis, partially filled with fluids analogous to spacecraft propellants, and tested at 50% and 75% fill ratios under varying angular velocities and accelerations. The comparative results demonstrated strong agreement between simulation and experiment. DNS predictions reproduced average centrifugal forces within 3–6% error and successfully captured key torque features, including peaks associated with Euler acceleration during spin-up and spin-down phases. Bubble oscillations observed during steady rotation were also replicated, with simulated oscillation frequencies deviating by less than 4% from measured values. Furthermore, higher fill levels were found to increase damping, thereby enhancing fluid stability.

Overall, the study reinforced the reliability of advanced numerical models in replicating complex fluid behaviours in microgravity. By validating DNS through the FLUIDICS experimental campaign, Dalmon et al. provided strong evidence that such modelling approaches can be applied with confidence to predict spacecraft propellant dynamics, supporting both mission planning and the design of slosh mitigation strategies.

To advance the modelling of sloshing in microgravity, several novel computational methods have been developed in recent years. Josip Bašić et al. [27] applied the Lagrangian Differencing Dynamics (LDD) method to simulate fluid sloshing under variable motion in reduced gravity. Unlike traditional grid-based techniques, LDD is a mesh-free, volume-conservative, second-order accurate approach that effectively captures free-surface breakup and complex fluid–structure interactions. In their study, the method was employed to model sloshing inside a tank undergoing non-uniform motion representative of spacecraft manoeuvres. Notably, the approach required only the vessel geometry and initial free-

surface configuration, eliminating the need for volumetric meshing, and was executed efficiently using GPU acceleration. Results confirmed LDD's capability to reproduce pressure and velocity fields under variable gravity with high fidelity, extending earlier validations conducted in constant gravity. These findings demonstrate the method's suitability for space applications involving transient fluid dynamics, with future extensions expected to incorporate surface tension and gas-phase interactions for more comprehensive modelling.

In a related development, Bole Ma et al. [28]. introduced an arbitrary Lagrangian–Eulerian finite element method (ALE-FEM) tailored for liquid sloshing in microgravity. A key innovation of their microgravity. Explicit treatment of contact angle hysteresis is often oversimplified or neglected in conventional models. By employing a highly refined contact-free-surface mesh, their approach distinguished between advancing and receding contact angles, thereby capturing the directional resistance at the contact line caused by surface imperfections or material properties. Validation against experimental data showed close agreement in predicting contact line height along the tank wall and free-surface elevation along the axis. When extended to spherical tanks, the study revealed that neglecting hysteresis produced significant discrepancies in free-surface dynamics, underscoring its critical role in governing interface behaviour under low gravity, where capillary effects can dominate system responses.

Beyond numerical developments, several studies have emphasized the impact of sloshing on spacecraft dynamics and control. Da Fonseca et al. [29] investigated Control Structure Interaction (CSI) in Low Earth Orbit (LEO) Launch Space Systems (LSS), with a focus on coupling between attitude/orbit control actions and structural flexibility. Their mathematical model incorporated flexible solar arrays and a water tank mounted on a tubular platform, with reaction wheels and thrusters providing actuation. Using equivalent spring–mass representations for the sloshing liquid and the assumed mode method for structural displacement, MATLAB simulations revealed that sloshing can significantly degrade spacecraft attitude stability, inducing residual oscillations and potentially destabilizing pointing systems.

The effects of sloshing during On-Orbit Refuelling (OOR) have also been examined. R. Sah, R. Srivastava [30], and co-workers developed a nonlinear dynamic model of propellant transfer between chaser and target spacecraft, combining a time-varying spring–mass–damper system for axial sloshing with a pendulum model for radial dynamics. Validation against CFD simulations in Open FOAM demonstrated less than 10% deviation, while requiring far fewer computational resources. This balance of accuracy and efficiency positions the model as a practical alternative to high-fidelity CFD for mission design and operational analysis.

Rotary sloshing in launch vehicles has likewise received renewed attention. Jeb S. Orr et al. [31] critiqued the limitations of linear spring–mass–damper models, showing that nonlinear effects, particularly rotary sloshing, can induce persistent oscillations and roll–coupling instabilities during ascent. By employing nonlinear representations such as the spherical pendulum and Bauer paraboloid models, validated against high-fidelity vehicle simulations, they demonstrated that even with ring baffles, rotary slosh-induced limit cycles may occur under large manoeuvres. These results highlight the necessity of integrating nonlinear slosh dynamics into flight control system design, especially for modern lightweight launch vehicles where inherent damping is reduced.

Finally, thermal effects have been increasingly recognized as inseparable from slosh dynamics. Monteiro et al. [32] performed controlled microgravity experiments aboard ESA's 83rd parabolic flight as part of the NT-SPARGE (Non-Isothermal Sloshing Parabolic Flight Experiment). Two identical cylindrical tanks, partially filled with HFE-7000, were employed: one under isothermal conditions, the other with a stratified temperature profile and

active pressurization. The experiments revealed that sloshing in the non-isothermal tank triggered boiling when liquid contacted the warmer upper walls, leading to unpredictable surface motions, thermal disruptions, and sharp pressure spikes. In contrast, the isothermal tank exhibited relatively stable dynamics. These results provide a rare dataset capturing the coupling between sloshing motion and thermal processes in microgravity, underscoring the need for integrated thermal–fluid models in cryogenic propellant management.

In his 2023 doctoral dissertation, Experiments and Simulations of Liquid Mass Gauging and Slosh Dynamics in Microgravity, Storey advanced the field of propellant management by integrating innovative sensing methods with unique spaceflight experiments [33,34]. His work addressed two key challenges: reliable mass gauging of cryogenic propellants in reduced gravity, and the accurate characterization of slosh dynamics under long-duration microgravity conditions. The first major contribution was the evaluation of Electrical Capacitance Tomography (ECT) as a non-intrusive diagnostic technique for liquid mass distribution in propellant tanks. ECT reconstructs the internal fluid configuration in real time by processing capacitance measurements between electrodes placed around the tank perimeter. Storey successfully demonstrated, for the first time, the operation of an ECT-instrumented tank under true microgravity, thereby assessing its feasibility for accurate mass gauging in realistic flight environments. This achievement represents an important step toward sensor-driven fluid management systems capable of operating without intrusive hardware.

The second major component of his research was the SPHERES-Slosh Experiment (SSE) aboard the International Space Station (ISS). The SPHERES platform (Synchronized Position Hold Engage and Reorient Experimental Satellites) consists of free-flying, basketball-sized satellites designed to evaluate guidance, navigation, and control algorithms in microgravity. Within SSE, fluid-filled tanks were manipulated by the SPHERES units to generate controlled, long-duration slosh events with precisely defined initial conditions. The campaign enabled the collection of synchronized video and six-degree-of-freedom inertial data, yielding a benchmark dataset for the validation of computational fluid dynamics (CFD) models of sloshing in reduced-gravity environments. Building on these experimental foundations, Storey introduced the concept of an ECT-based "slosh sensor." Unlike traditional analogue spring–mass approximations or computationally intensive CFD models, this sensor concept reconstructs sequential three-dimensional liquid volumes and estimates velocity fields in near real time. By providing direct estimates of fluid forces and torques, such a system could enable onboard detection and control of slosh-induced disturbances without excessive computational burden.

Overall, Storey's work represents a significant advance toward sensing-driven, real-time control of sloshing phenomena, offering a pathway to safer and more efficient spacecraft propellant management. His integration of ECT with the ISS-based SSE campaign provides both a novel diagnostic capability and a uniquely valuable dataset for model validation, with broad implications for future spacecraft design and operations.

In microgravity environments such as aboard the International Space Station (ISS), bubbles in a sloshing tank emerge from the complex interaction of liquid and vapour phases during fluid motion. When the liquid encounters warmer boundaries such as the tank's top wall localized boiling can occur, particularly under thermally stratified conditions. In contrast to terrestrial environments, the absence of buoyancy prevents bubbles from rising and coalescing, allowing them to persist and disperse throughout the liquid volume. Rapid accelerations and interface collapses during sloshing may also entrap vapour pockets, further contributing to bubble formation and highlighting the challenges of phase separation in cryogenic propellant systems [35].

Analogous insights into bubble behaviour have been obtained in the realm of quantum fluids. Carollo et al. [36] reported the formation of ultracold atomic bubbles in orbital microgravity using NASA's Cold Atom Laboratory on the ISS. By applying a radiofrequency-dressing technique, they generated stable bubble-shaped configurations in ultracold atomic gases, with the potential for Bose–Einstein condensation. This experimental platform enabled the investigation of bubble thermodynamics under unprecedented conditions, revealing significant cooling effects during bubble inflation and novel dynamics of shell-like quantum structures.

Together, these studies illustrate the diverse and often counterintuitive phenomena associated with bubbles and vapour dynamics in microgravity—from persistent vapour pockets in cryogenic propellants to emergent quantum states in ultracold fluids. Both examples highlight how the absence of buoyancy fundamentally alters the mechanisms of energy storage, transfer, and dissipation within multiphase systems. These effects provide unique opportunities not only for advancing fundamental fluid physics but also for improving energy-efficient cryogenic management strategies critical to future space missions.

Because access to sustained microgravity remains limited and expensive, sloshing dynamics are typically investigated using short-duration experimental platforms that approximate weightlessness. Parabolic flights, offering 15–25 s of reduced gravity, are widely employed to visualize free-surface motion and quantify energy damping and transfer during oscillations. Drop towers extend exposure to several seconds of high-quality microgravity by releasing sealed capsules in free fall, enabling precise measurements of interface deformation, bubble motion, and slosh-induced pressure fluctuations—key contributors to viscous and interfacial energy loss. For longer observation windows, sounding rockets provide minutes of microgravity and have been used to capture the evolution of vapour–liquid distribution and thermally driven dissipation in cryogenic systems.

Ground-based simulators such as clinostats and random positioning machines reproduce certain diffusion-dominated aspects of microgravity by continuously altering tank orientation. However, they cannot replicate realistic inertial coupling or slosh-induced energy pathways, making them unsuitable for studying dynamic fluid oscillations and damping behaviour. While these facilities remain valuable for validating isolated thermophysical phenomena, they fall short of reproducing the nonlinear energy conversion between mechanical motion, heat transfer, and phase change that defines cryogenic sloshing in orbit.

Collectively, these experimental surrogates have been instrumental in validating computational models and advancing understanding of fluid–structure–thermal energy coupling. Yet their limited duration leaves open a critical frontier: the long-term evolution of sloshing-induced energy dissipation, vapour entrapment, and boil-off acceleration under continuous microgravity. Over mission-relevant timescales, trapped vapour pockets modify effective damping and redistribute energy between mechanical and thermal modes, directly linking sloshing dynamics to propellant energy loss and boil-off rates.

Addressing these challenges requires extending research into orbital testbeds capable of capturing the full energy-dissipation spectrum over sustained operation periods. Equally important is the co-design of active thermal control systems such as thermodynamic venting (TVS) and zero-boil-off (ZBO) technologies with structural damping mechanisms like composite baffles. Such integrated strategies would simultaneously stabilize the liquid interface, enhance thermal uniformity, and suppress slosh-induced energy losses, forming the foundation for high-efficiency, long-duration cryogenic propellant storage essential for lunar, Martian, and deep-space missions.

Critical Synthesis of Sloshing in Microgravity

The body of literature on microgravity sloshing reveals a progressive evolution from simplified analytical analogues toward data-driven, multi-physics, and energy-aware frameworks. Early analytical models such as linear spring–mass analogues provided initial insight into propellant motion but failed to capture how mechanical oscillations transform into heat, vapour generation, and energy loss under reduced gravity. Orr et al. demonstrated that linear models could not predict rotary sloshing instabilities even in baffled configurations, exposing their inability to represent nonlinear energy exchange and dissipation mechanisms that dominate low-gravity environments.

Modern computational methods—Direct Numerical Simulation (DNS), Arbitrary Lagrangian–Eulerian Finite Element Methods (ALE-FEM), and Lagrangian Differencing Dynamics (LDD) now resolve these phenomena with much greater fidelity. Bašić showed that LDD can efficiently reproduce free-surface breakup and viscous damping, while Ma et al. highlighted ALE-FEM's strength in resolving contact-angle hysteresis and thermally driven interfacial deformation, both of which govern energy transfer between surface tension, inertia, and heat flux. However, trade-offs persist: GPU-accelerated LDD achieves computational efficiency at the cost of excluding capillary energy effects, whereas ALE-FEM remains computationally prohibitive despite its thermodynamic completeness. This recurring compromise reflects a central challenge in sloshing research—balancing numerical efficiency with accurate representation of energy dissipation and conversion under mission-relevant conditions.

Validation of these models relies heavily on orbital experiments that measure real energy loss and damping rates. Campaigns such as FLUIDICS (Dalmon et al.) and SPHERES-Slosh (Storey et al.) aboard the ISS provide benchmark data for tracking kinetic-to-thermal energy conversion, pressure fluctuations, and interfacial damping coefficients. In contrast, terrestrial surrogate parabolic flights, drop towers, and sounding rockets remain essential for calibration but are limited by seconds-long microgravity durations. They capture only the early stages of energy redistribution and phase-change onset, not the cumulative effects that govern long-term propellant stability. Consequently, sustained on-orbit testing remains indispensable for understanding how energy dissipates and re-enters the thermal domain during long-duration missions.

A persistent research gap lies in quantifying the coupled energy feedback between sloshing, damping, and boil-off acceleration during extended microgravity storage. Over time, trapped vapour bubbles modify viscous and capillary damping pathways, amplifying thermal stratification and pressurization energy. Current approaches often treat sloshing control and thermal management as independent problems, yet both define a single energy loop: oscillatory kinetic energy becomes internal energy through viscous losses, which then drives vaporization and mass loss. Future spacecraft must instead adopt co-designed architectures, coupling structural energy dissipation hardware (e.g., composite baffles) with active energy recovery and control systems such as Thermodynamic Venting Systems (TVS) and Zero-Boil-Off (ZBO) cryocoolers. These integrated frameworks could stabilize free-surface motion while simultaneously reclaiming or redirecting excess thermal energy, achieving both slosh damping and propellant energy efficiency.

A comparative review of Technology Readiness Levels (TRLs) further clarifies this energy-centric landscape. At higher TRLs, simplified mechanical models endure because of their reliability in controller design, despite their neglect of thermal energy pathways. Mid-TRL research focuses on CFD-based prediction of damping coefficients and heat-flux coupling, while low-TRL innovations explore experimental frontiers such as Romero-Calvo's magnetic ferrofluids for active energy-based slosh suppression, Storey et al.'s ECT sensors for real-time dissipation mapping, and the development of thermo-functional composite

baffles that absorb, redirect, or radiatively dissipate energy. Although experimental, these concepts embody the field's shift toward energy-integrated, microgravity-resilient systems.

In synthesis, the literature reflects a decisive transformation from passive containment toward adaptive energy-management architectures. Early hardware such as slat screens (Nadeem et al.) offered limited, context-dependent energy damping, whereas emerging paradigms converge on sensing, modelling, and structural control systems that collectively predict, monitor, and dynamically minimize sloshing-induced energy losses. This convergence—linking fluid dynamics, structural mechanics, and thermodynamics into one coupled energy framework—marks both the greatest technical challenge and the most promising pathway toward high-efficiency, long-duration cryogenic operations in deep space.

4. Thermodynamic Effects on Cryogenic Sloshing

Sloshing in cryogenic propellant tanks cannot be regarded as a purely mechanical process; it is an energy conversion phenomenon governed by the coupled thermodynamic interactions between the liquid, vapour, and tank structure. Even minor surface disturbances modify local heat flux, temperature gradients, and phase-change processes such as evaporation, condensation, and film boiling transforming mechanical agitation into irreversible thermal losses. Because cryogens exhibit low thermal conductivity, high latent heat of vaporization, and strong temperature-dependent variations in density, viscosity, and surface tension, these disturbances strongly influence energy dissipation mechanisms. The resulting feedback modifies vapour pressure, interfacial tension, and density distribution, altering oscillation frequencies, damping behaviour, and free-surface stability.

In normal gravity, inertia-driven oscillations dominate the energy transfer, where sloshing converts mechanical input into turbulent mixing and convective heat exchange. Studies show that increased sloshing acceleration and higher fill ratios amplify both dynamic pressure fluctuations and heat generation. Xue et al. [37] demonstrated that higher excitation intensifies pressure oscillations, while Sun et al. [38] reported that reduced fill levels—though lowering hydrodynamic load—raise vapour temperature and pressure, doubling boil-off gas (BOG) losses at amplitudes of roughly 2 m. Similarly, Le et al. [39] observed that abrupt motion cessation induces pressure collapse via rapid condensation on subcooled surfaces, and Liu et al. [40–42] found that prolonged agitation yields chaotic condensation and asymmetric interfacial decay, with 60% fill conditions marking peak instability where mechanical and thermal losses reinforce each other [43].

Under reduced or microgravity, the energy dissipation pathway shifts from bulk convection to surface-tension-controlled interfacial transport. The absence of buoyancy allows vapour films and bubbles to persist [44], disrupting equilibrium and promoting local condensation and asymmetric pressure variations. Wang et al. [45] showed that spherical tanks reduce total heat ingress and BOG generation, while Zuo et al. [46] found that thermodynamic vent systems operate more efficiently in microgravity as vapour–liquid mixing enhances condensation. Conversely, Liu et al. [47] reported that stratification develops more slowly in rotating tanks, yet even small oscillations can cause strong vapour condensation and temperature oscillations, reinforcing stratification as observed by Zhan Liu et al. [48]. Thus, while the mechanisms differ, sloshing remains a key source of thermal and pressure instability across gravitational regimes.

Across both environments, the coupling between phase change and thermodynamics defines the main channel of energy loss [49]. Heat ingress drives self-pressurization and stratification [50,51], while slosh-induced convection accelerates evaporation and BOG generation. Passive mitigation techniques—low-conductivity composite walls and internal baffles—reduce both heat ingress and slosh-induced mixing [52], and advanced insulation,

such as vapour-cooled shields or fibre–vacuum–deposited multilayer insulation, cuts total heat leakage by nearly 50% [53]. When these are insufficient, active systems such as thermodynamic venting [54], gas bubbling [55], or cryocoolers [56] are required. Neglecting phase-change effects in models leads to underestimation of ullage pressure by over 18% [57]. Large-scale systems further exhibit dominant surface evaporation over bulk boiling [58], and even trace contamination modifies stratification and BOG behaviour [59], while ascent heating adds further thermodynamic stress [60,61].

Despite significant progress, predictive energy-dissipation modelling remains computationally demanding. Fully coupled thermo-fluid simulations are rarely feasible for real-time control, highlighting the need for reduced-order models (ROMs) that preserve nonlinear energy coupling for use in digital twins. Long-term effects of aging and contamination on coupled thermodynamics also remain poorly characterized. To close these gaps, large-scale and long-duration validation experiments are required to quantify how mechanical excitation energy is partitioned into turbulence, thermal storage, and irreversible vaporization.

Overall, thermodynamic coupling and phase change from the unifying thread of energy dissipation in cryogenic sloshing. In normal gravity, inertia-driven motions amplify heat and pressure oscillations, while in microgravity, capillary and film-dominated dynamics govern interfacial stability. Integrating validated Multiphysics and reduced-order frameworks into digital-twin architectures will enable adaptive control of slosh-induced energy loss, advancing the design of lighter, safer, and more energy-efficient cryogenic systems for long-duration aerospace missions [62,63].

Critical Synthesis of Thermodynamics Effects in Cryogenic Sloshing

A comprehensive synthesis of thermodynamic effects in cryogenic sloshing reveals a system defined by a strong dichotomy between normal- and microgravity environments and stratified by distinct gradients of technological maturity. In normal gravity, there is broad consensus that inertia-driven oscillations accelerate energy dissipation through amplified pressure fluctuations, chaotic condensation, and enhanced boil-off gas (BOG) generation. The process converts mechanical sloshing energy into thermal and latent energy, reducing overall propellant efficiency. Yet, the literature is not without nuance: while most studies depict sloshing as inherently detrimental, some experiments indicate that intermittent or low-amplitude oscillations can promote controlled condensation and gentler pressure decay—acting as stabilizing dissipative mechanisms under constrained conditions. Despite its maturity, this research domain remains constrained by methodological simplifications; most experimental work employs idealized sinusoidal or single-axis excitations, which fail to replicate the stochastic, multi-axis forcing characteristic of actual launch and orbital operations. Nonetheless, normal-gravity models are supported by extensive ground-based validation and operational flight data, corresponding to high TRLs (6–7).

By contrast, the reduced- and microgravity regime remains low-TRL (3–4) and less experimentally mature, governed primarily by surface-tension–driven interfacial dynamics. Here, energy dissipation manifests through capillary waves, vapour film formation, and asymmetric condensation cycles—phenomena often counterintuitive to terrestrial intuition. For example, thermodynamic vent systems (TVS) have been observed to perform more efficiently in microgravity due to enhanced vapour–liquid mixing and rapid condensation of superheated vapour, while natural stratification proceeds more slowly owing to the absence of buoyancy. Yet, sloshing remains a powerful destabiliser: even weak oscillations in LH_2 tanks can induce asymmetric condensation, pressure collapse, and sharp temperature fluctuations, compounding stratification over long durations. These findings illustrate

that, although sloshing and phase change jointly govern energy conversion pathways, our understanding of their coupling in low-gravity environments remains fragmentary due to short-duration testing and the lack of long-term orbital validation.

Across both regimes, one principle is universally acknowledged: accurate treatment of phase change as an energy dissipation mechanism is indispensable. Neglecting evaporation or condensation can inflate ullage pressure predictions by nearly 20%, compromising mission-critical design margins. This recognition exposes a central engineering tension—between high-TRL passive systems (e.g., multilayer insulation, vapour-cooled shields, composite walls) that ensure reliability but offer limited adaptability, and emerging active systems (e.g., TVS, cryocoolers, destratification bubbling) that enable dynamic thermal control but at higher mass and power cost. This trade-off defines the current frontier between static and adaptive energy management in cryogenic systems.

The path forward requires a dual trajectory: (1) advancing experimental infrastructure through full-scale, instrumented testbeds in both gravity regimes and extended on-orbit demonstrations to bridge the persistent validation gap, and (2) developing reduced-order and physics-informed models (PINNs) that preserve nonlinear coupling between sloshing, heat transfer, and phase change while remaining computationally tractable. Embedding these models within digital-twin architectures would enable real-time tracking of dissipative losses, predictive boil-off control, and autonomous venting optimization. Such frameworks represent a shift from descriptive modelling toward active energy management, transforming cryogenic tanks into adaptive systems capable of minimizing energy loss in real time.

Ultimately, while inertia-driven dynamics dominate in normal gravity and surface-tension physics define microgravity, the coupling of thermodynamics and phase change remains the unifying energy pathway governing pressurization, damping, and long-term stability. Addressing this continuum—through experimental maturity and model fidelity will elevate current low-TRL microgravity understanding to flight-proven reliability. Success in this endeavour will unlock the next generation of cryogenic propellant systems: lighter, safer, and more energy-efficient architectures capable of sustaining lunar, Martian, and deep-space operations.

5. Sloshing of Liquid in Composite Overwrapped Pressure Vessels

The inherent advantages of Composite Overwrapped Pressure Vessels (COPVs) in modern launch vehicles and spacecraft—primarily their superior strength-to-weight ratio and high-pressure tolerance for cryogenic propellants—are significantly counterbalanced by complex challenges that extend beyond simple dynamic loading. The combined effects of sloshing, extreme cryogenic temperatures, and the unique anisotropic nature of COPV materials create a multifaceted threat to structural integrity and mission reliability.

During dynamic phases such as liftoff, stage separation, or critical attitude control manoeuvres, the partially filled cryogenic liquid within COPVs is highly susceptible to sloshing. This phenomenon introduces a cascade of detrimental effects: unsteady pressure loads, complex fluid–structure interactions, and severe disturbances to thermal equilibrium. Unlike the more forgiving isotropic behaviour of traditional metallic tanks, the anisotropic mechanical properties of COPVs make them uniquely vulnerable. Asymmetric sloshing impacts do not merely distribute stress; they can cause highly localized stress amplifications that concentrate forces in specific directions, potentially leading to localized delamination, liner buckling, or even catastrophic failure in areas that might otherwise appear robust.

Compounding these dynamic challenges are the critical thermo-mechanical interactions intrinsic to cryogenic storage. Repeated boil-off cycles, a necessity for managing propellant pressure, and the agitation caused by sloshing collaboratively induce signifi-

cant thermal cycling stress. This cycle of cooling and warming, often localized and rapid, stresses the interface between the polymer liner and the composite overwrap. Localized cooling can lead to condensate formation, exacerbating temperature gradients and promoting material degradation. In regions with even minor manufacturing defects—such as imperfect bonding, voids, or material heterogeneity—these thermal stresses are magnified. The polymer liner, typically designed for flexibility, can undergo cryogenic embrittlement, lose its ductility and become prone to microcracking. Simultaneously, the composite overwrap can experience matrix–fibre debonding, where the resin matrix separates from the high-strength fibres, and further microcracking within the matrix itself. This degradation compromises the load-bearing capacity and sealing function of the COPV.

Furthermore, the long-term exposure to cryogenic propellants introduces insidious chemical and physical degradation mechanisms. Hydrogen diffusion, particularly with propellants like liquid hydrogen, can infiltrate the resin matrix of the composite, leading to plasticization or embrittlement of the polymer chains. This chemical attack, combined with sustained temperature gradients across the vessel wall, can further weaken the critical interface between the liner and the composite fibres. This gradual degradation diminishes the vessel's ability to withstand both operational pressures and dynamic slosh-induced loads, potentially leading to slow leaks, reduced burst pressure capability, or sudden structural failure over the mission lifetime.

Recent investigations into sloshing dynamics in composite vessels have further emphasized the role of structural anisotropy in influencing fluid–structure interactions. Pratik Tiwari et al. [64] developed a robust three-dimensional finite element formulation to analyze sloshing in partially filled laminated composite cylindrical tanks under external excitations, using a direct coupling method for efficient fluid–structure interaction. Their work employed degenerated shell elements for the composite tank and 20-noded brick elements for the fluid domain, validated through both literature comparisons and experimental results.

Their findings emphasize that radial stiffness, rather than overall structural stiffness, plays a dominant role in sloshing suppression. This insight is particularly valuable for COPV design, where ply orientation can be tailored to enhance performance under dynamic loading. The study revealed that optimized ply orientations can significantly reduce slosh height, even allowing thinner tank walls to outperform thicker configurations with suboptimal layups. This aligns with the growing emphasis on customizing composite architecture to not only meet mechanical strength requirements but also minimize dynamic instabilities like sloshing.

Expanding on the complexities of sloshing dynamics in composite structures, Mahdi Karimi et al. [65] investigated the free vibration behaviour of vertically oriented composite laminate plates coupled with sloshing fluids. Their work introduces both hybrid composite laminates (HCL), composed of multiple fibre types, and variable stiffness composite laminates (VSCL), featuring curvilinear fibre paths, as structural configurations interfacing with sloshing liquid. Using Reddy's shear deformation plate theory combined with the Rayleigh–Ritz method, they formulated a fluid–structure interaction (FSI) model that accounts for both sloshing and bulging fluid modes, emphasizing the critical role of fibre orientation and laminate tailoring on vibrational response. This study is particularly relevant to COPVs, where composite behaviour is highly dependent on layup design and fibre alignment. Karimi et al.'s [65] findings demonstrate that VSCL and HCL configurations can significantly widen the spectrum of natural frequencies, enabling more flexible and targeted design strategies for dynamic environments. Importantly, such fibre architecture modifications not only influence stiffness and damping properties but also affect how sloshing energy is absorbed or amplified at the structural interface.

Furthermore, P. Pal et al. [66] took a unique approach by using a meshless method, specifically the meshless local Petrov–Galerkin (MLPG) technique, to study sloshing in partially filled rectangular composite containers. Instead of relying on traditional mesh-based models, their method used a more flexible, point-based system to calculate pressure changes and fluid motion, which is especially useful for handling complex interactions like fluid–structure coupling. They explored how different fibre orientations and wall thickness affect the way the liquid moves and how much stress it puts on the tank walls. One key takeaway was that composite tanks with thinner walls or certain ply orientations can experience much stronger sloshing-induced vibrations, which is important when thinking about cryogenic applications where structural integrity is already at risk from thermal stress and potential embrittlement. Their method also gives a peek into the future of 3D slosh modelling for more complex tank geometries, like those found in COPVs, where understanding localized stress and pressure buildup could make all the difference in preventing damage during critical phases like launch or maneuvering.

Furthermore, Dong-Hyeop Kim et al. [67] conducted a comprehensive numerical investigation into the impact-induced damage behaviour of a composite fuel tank assembly, particularly under drop impact conditions relevant to helicopter applications. Utilizing a Coupled Eulerian–Lagrangian (CEL) method, the study incorporated fluid–structure interaction (FSI) analysis to account for the dynamic interplay between the sloshing liquid fuel and the composite tank structure. The Hashin failure criteria were applied to evaluate structural failure, enabling the characterization of various composite damage modes.

Key parameters such as the amount of fuel and drop impact angle were varied to assess their influence on structural integrity. The results indicated that while sloshing itself did not significantly contribute to damage, an increased fuel volume led to greater impact energy transmission to the tank, thereby aggravating the extent and severity of damage. Similarly, oblique impact angles introduced localized stress concentrations, particularly near the tank edges, further exacerbating structural failure. On the other hand, design features such as foam core layers and reinforced lower edges were shown to effectively absorb impact energy, mitigating damage to some extent. The findings provide valuable insights for the design and certification of composite fuel tank assemblies, especially in the context of airworthiness assessments and drop impact test planning. The methodology demonstrated and observed failure trends serve as a useful reference for enhancing the safety and resilience of fuel systems in rotary-wing aircraft.

In addition, Dipak K. Maiti et al. [68] developed a 3D finite element model to analyze sloshing frequencies in partially filled cylindrical laminated composite containers, focusing on fluid–structure interaction. Using Reissner–Mindlin theory and the Helmholtz wave equation, they accurately captured the coupled dynamics between the composite tank and the sloshing fluid. Their parametric study showed that ply orientation, tank geometry, and fill level significantly affect natural sloshing frequencies, with the $(0/45)_{2s}$ layup offering the highest frequency. The model is validated and serves as a reliable, efficient tool for studying composite tank sloshing under dynamic conditions.

In addition, E. Kormanikova et al. [69] developed a multiscale model to analyze liquid-filled laminated composite cylindrical tanks. Using a hexagonal microstructure model and numerical homogenization, they derived the effective properties of the composite. The study emphasized the importance of laminate layup and material anisotropy in influencing fluid–structure interaction, particularly the pressure effects of sloshing fluid on tank walls.

Similarly, Hamid Reza Moghaddasi et al. [70] explored the nonlinear dynamics of simply supported, thin laminated circular cylindrical shells coupled with large amplitude sloshing fluid. Using the Flügge–Lure–Byrne nonlinear shell theory and potential flow theory for the fluid domain, they analyzed the interaction between shell deformation

and nonlinear sloshing, particularly under harmonic excitation. Their findings reveal that nonlinear sloshing reduces the beating effect in the shell's response but increases radial deformation compared to linear models. The study also shows that for flexible shells, nonlinear sloshing notably alters the frequency–response curves, especially at higher fluid fill levels, while having minimal impact on the free surface profile. Conversely, in stiffer shells, the dynamic response is less sensitive, but the fluid surface elevations are significantly affected. This work emphasizes the importance of considering nonlinear sloshing effects in the vibration analysis of fluid-filled laminated shell structures.

In the same vein, Sirwan Farhadi et al. [71] conducted a hydrostatic vibration analysis of laminated composite rectangular plates partially in contact with fluid. Using the Rayleigh–Ritz method and shear deformation theories, they showed that fluid–structure interaction significantly alters natural frequencies and mode shapes. Results revealed that increasing fluid depth lowers frequencies, while increasing plate thickness, tank width, or clamped constraints raises them. Fibre orientation and aspect ratio also notably affect the vibrational response.

While traditional sloshing studies have emphasized short-term control in single-flight missions, the rise of reusable launch vehicles demands a broader framework that explicitly considers cumulative deformation and fatigue under repeated cryogenic cycling. Sustained exposure to sloshing loads, coupled with steep thermal gradients, introduces long-term risks such as progressive shell deformation, micro-crack initiation in composite overwrapped pressure vessels (COPVs), and performance loss in composite baffles.

Recent investigations reveal that nonlinear vibrations in cantilevered cylindrical shells containing cryogenic fluids not only alter mechanical response but also modulate energy transfer pathways within the tank structure. At high fill levels, vibration modes transition from softening to hardening behaviour, reflecting a redistribution of mechanical energy between the fluid and structural modes. In thin-walled shells, intensified thickness deformation amplifies internal friction and viscous dissipation, demonstrating that classical small-amplitude sloshing theory is insufficient for reusable cryogenic tanks. These nonlinear effects convert oscillatory kinetic energy into localized heating and cyclic stress accumulation, directly influencing fatigue life and thermal energy buildup within the structure. Consequently, fatigue assessments must integrate nonlinear fluid–structure interaction (FSI) with repeated-cycle thermomechanical analysis—particularly for composite overwrapped pressure vessels (COPVs) where cyclic stresses and thermal gradients evolve concurrently.

Parallel studies examining sloshing under realistic seismic and launch excitations using turbulence-based and multiphase CFD models further confirm that energy dissipation efficiency depends on excitation frequency, fill ratio, and structural coupling. Low-frequency, high-energy events generate the most violent free-surface oscillations, with strong wave–wall impacts driving rapid mechanical-to-thermal energy conversion. The geometry of internal baffles emerges as a decisive control factor: combined horizontal–vertical configurations maximize damping efficiency and wave energy attenuation, while purely planar or perforated geometries exhibit uneven dissipation patterns. Yet, experimental evidence shows that baffle effectiveness degrades over time as thermal cycling and repeated mechanical stresses reduce structural damping, lowering the system's overall capacity to absorb and dissipate sloshing energy.

Collectively, these findings highlight that sloshing-induced deformation, cyclic fatigue, and energy dissipation degradation are interdependent phenomena governing the durability of cryogenic tanks. Sustainable tank design therefore demands an integrated modelling framework that unites nonlinear FSI, fatigue-life prediction, and energy dissipation analysis under repeated cryogenic cycling. Simultaneously, baffle systems must be engineered for

energy endurance—optimizing both wave damping and thermal resilience over multiple operational cycles. Recognizing sloshing as both a structural and thermodynamic energy process reframes it as a key driver of efficiency, reusability, and certification standards for next-generation cryogenic aerospace systems.

Critical Synthesis of Liquid in COPVs

Recent research on sloshing within composite cryogenic overwrapped pressure vessels (COPVs) has converged on a key understanding: the anisotropic stiffness and damping characteristics of composite laminates directly govern energy transfer and dissipation during dynamic fluid–structure interaction. Unlike metallic tanks, whose isotropy simplifies the mechanical response, composite structures exhibit direction-dependent stiffness that redistributes vibrational energy through the laminate architecture. Studies by Tiwari et al. and Karimi et al. demonstrate that optimizing ply orientation, stacking sequence, and hybridization can significantly reduce sloshing-induced energy amplification and structural resonance, thereby enhancing damping efficiency. However, this consensus is tempered by alternate findings from Kim et al., who show that under impact or high-energy excitation, fluid inertia contributes more strongly to total energy input than resonance itself—implying that energy dissipation mechanisms must be tuned not only to material anisotropy but also to excitation spectrum. Similarly, Moghaddasi et al. establish that nonlinear shell–fluid coupling governs both energy absorption and re-radiation, challenging the adequacy of classical linear FSI formulations that neglect these conversion dynamics.

From a technology readiness standpoint, numerical and experimental frameworks can be categorized by their ability to capture and quantify energy pathways. High-TRL models, such as FEM-based FSI solvers, provide validated predictions of structural loads but typically treat material damping as static, overlooking evolving dissipative behaviour under repeated cryogenic cycling. Mid-TRL approaches—like meshless particle methods and hybrid laminate concepts offer richer representation of wave impact energy transfer and fracture-induced dissipation, though their validation remains limited. At the low-TRL frontier, emerging Multiphysics models attempt to integrate thermal energy accumulation, sloshing-induced vibration, and progressive stiffness degradation; while computationally intensive, they offer a glimpse into fully coupled thermo-mechanical fatigue frameworks essential for reusability design.

This TRL gradient reveals a critical knowledge gap: while short-term sloshing-energy dynamics are increasingly understood, long-term energy degradation mechanisms remain poorly characterized. Existing models seldom capture how cyclic cryogenic exposure alters internal damping, fracture toughness, or interlaminar conductivity factors that dictate how efficiently a COPV can dissipate sloshing energy over thousands of cycles. Addressing this gap demands the development of lifecycle-based Multiphysics models coupling nonlinear FSI with cryogenic fatigue and energy dissipation maps derived from experimental data.

Embedding these frameworks into digital twin architectures would enable real-time tracking of sloshing-induced energy loss, stiffness decay, and damage accumulation—transforming COPV sloshing analysis from a static load assessment into a predictive, energy-centric reliability model. Such integration will be pivotal for next-generation reusable cryogenic stages, where energy dissipation efficiency directly underpins structural longevity, propellant stability, and mission reusability.

6. Experimental and Numerical Investigation of Cryogenic Sloshing Dynamics

Recent studies have increasingly adopted a sophisticated suite of numerical techniques to unravel the highly coupled thermal–fluid behaviour of cryogenic sloshing, a challenge at the nexus of fluid dynamics, heat transfer, and phase change. Among these, the Volume of Fluid (VOF) method remains the engineering workhorse, valued for robustness in interface tracking and relatively low computational cost. For example, Ryu et al. showed that VOF predicted a 66% increase in (BOG) in an LH_2 tank under 3 Hz excitation, consistent with LNG mixing studies by Grotle & Æsøy. However, validation against drain-down experiments has revealed systematic overprediction, with Baker & Hauser reporting a ~25% higher condensation rate than measured. This limitation arises from numerical diffusion in the Eulerian grid, which smears steep gradients and reduces accuracy in overturning waves or jet fragmentation.

To address these weaknesses, meshless Lagrangian methods such as Smoothed Particle Hydrodynamics (SPH) and Moving Particle Semi-implicit (MPS) have gained prominence. By tracking discrete parcels, they excel at capturing violent, chaotic free-surface motion. Freeman demonstrated that SPH reproduced slosh amplitudes within ±10% of shaking-table experiments, compared to VOF's 20–25% deviation. Likewise, Huang et al. showed MPS captured spherical LNG tank pressure peaks more accurately than VOF, particularly under steep wave impacts. The trade-off, however, is computational demand ~5× higher than VOF, limiting their TRL to mid-range design studies.

For problems where fluid–structure interaction (FSI) is critical, Coupled Eulerian–Lagrangian (CEL) methods are preferred. Ryali et al. employed CEL in ABAQUS to simulate LH_2 tanks with baffles, capturing not only BOG growth but also wall stresses exceeding 4 MPa and baffle deformation absent in CFD-only approaches. Similarly, Ma & Zhang used an ALE formulation to reproduce rotary nonlinear sloshing in Cassini-type tanks, validating numerical resonance predictions against experiment with <8% error. These methods provide a richer picture of tank survivability but remain setup intensive.

At the apex of fidelity, Direct Numerical Simulation (DNS) resolves turbulence without modelling assumptions. Martinez et al. showed that DNS of LH_2 tanks predicted sloshing could increase condensation by ~40% relative to quiescent cases. While this provides benchmark-quality physics, DNS requires >100× the computational effort of VOF, confining its role to fundamental research rather than engineering design cycles.

A consistent outcome across all methods is that sloshing accelerates BOG generation by 20–80%, depending on excitation frequency, amplitude, and ullage composition. This behaviour can be rationalized by a mass-balance model:

$$\dot{m}_{BOG} = \frac{Q_{slosh}}{h_{fg}},\ Q_{slosh} = hA\Delta T + \rho C_P u' \Delta T \tag{15}$$

where $hA\Delta T$ represents enhanced wall heat flux due to splashing and $\rho C_P u' \Delta T$ captures convective mixing at the ullage–liquid interface. The table below summarizes key recent studies, highlighting this diversity of computational methods and their respective advantages in tackling specific facets of the sloshing problem. Table 1A–C present experimental, numerical, and hybrid approaches, clarifying the regimes where each is most effective.

Table 1. (**A**) Overview of Recent Experimental Methods for Cryogenic Sloshing Dynamics. (**B**) Overview of Recent Numerical Methods for Cryogenic Sloshing Dynamics. (**C**) Overview of Recent Hybrid (Experimental + Numerical Methods for Cryogenic Sloshing Dynamics).

Author Year	Method	Capability/Summary
	(A)	
Myrillas et al.	Shaking table (Exp.)	Internal obstructions reduce seismic sloshing peaks in LBE surrogates [72].
Simonini et al.	PIV (LN_2)	Tracer imaging of LN_2 flow/interface; resolves local velocities and interface motions [73].
Han et al.	Heat-exchanger tests (Exp.)	~55% heat-transfer drop at 12° roll (round tubes); geometry strongly affects performance [74].
	(**B**)	
Ryu et al.	VOF + phase-change	BOG ~66% at 3 Hz; vibration boosts heat transfer in LH_2 tanks [75].
Grotle & Æsøy	Modified Open FOAM	Validated pressure-drop correlations in LNG sloshing–mixing cases [76].
Duan et al.	CFD + theory	Resonance increases LNG vapour condensation & depressurization [77].
Zhu et al.	CFD	Peak force ~3.89 kN (5 g); large LH_2 slosh can invert free surface [78].
Ma & Zhang	CFD	Frequency & acceleration raise condensation rates; interface growth dynamics [79].
Hauser et al.	FLUENT (RANS)	Turbulence modelling improves pressure tracking in LN_2 tanks [80].
Sun et al.	VOF (with flow visualization)	Identified optimal anti-sloshing designs for offshore LNG heat-exchangers [81].
Sreeraj & Anbarasu.	Sigma-transform PF	Efficient for low–medium wave steepness without re-meshing [82].
Kang et al.	3D VOF	In LH_2 tanks, higher forcing frequency instability; low-energy slosh cools bulk [83].
Zhang et al.	Euler–AIAD	LOX slosh evaporation via kinetic thermal conversion [84].
Ma et al.	FEM (ALE)	Captures rotary nonlinear sloshing in Cassini tank; validated vs. reference data [85].
Freeman et al.	SPH	Effective for cylindrical tanks under multi-frequency forcing [86].
Chen et al.	VOF + UDF	Sloshing accelerates LNG rollover in large membrane tanks [87].
Liu et al.	VOF + UDF	Intermittent excitation in LOX pressure fluctuations, vapour drop [88].
Huang et al.	MPS	Accurate nonlinear sloshing in spherical LNG tanks [89].
Ryali et al.	CEL (ABAQUS)	LH_2 baffle effects on boil-off, wall stress, bubble growth [90].
Li, L. et al.	Tank-InterFoam (Open FOAM)	Arbitrary excitation; VOF phase-change modelling for LNG [91].
Li, C. et al.	VOF + mesh motion	Near-resonance sloshing pressure and BOG in Type-B tanks [92].
Meng et al.	FLUENT + dynamic mesh	Identified periodic slosh thresholds in two-phase LNG flow [93].
Martinez et al.	DNS (CLSVOF)	Sloshing boiling and self-pressurization in LH_2; high fidelity [94].
Baker & Hauser.	FLUENT	Over-prediction of slosh phase-change in methane vs. static drain benchmark [95].

Table 1. *Cont.*

Author Year	Method	Capability/Summary
	(**B**)	
Rahbarimanesh et al.	DNS (HEM cavitation)	LNG cavitation via Kelvin–Helmholtz vortex pairing; 3D instability [96].
Yang et al.	FVM vs. LBM	LBM ~14× faster than FVM with comparable accuracy [97].
	(**C**)	
Li et al.	SPH + experiment	Bubble-point instability reduces velocity (~25%); SPH shows ~1.3 mm inward damping [98].
Chen et al.	VOF + R134a exp.	Sloshing convection & BOG in membrane LNG tanks [99].
Grotle & Æsøy.	Bond-graph + exp.	Sloshing accelerates thermal response beyond PBU capacity [100].

Critical Synthesis of Experimental and Numerical Methods for Cryogenic Sloshing Dynamics

Recent investigations into cryogenic sloshing reveal a structured methodological hierarchy, with broad agreement on its adverse thermal consequences but persistent divergence in predictive reliability and physical interpretation. At the system level, there is near-universal consensus that sloshing amplifies (BOG) generation through enhanced convective mixing and wall impingement, often accelerating mass loss by 20–80% relative to quiescent tanks (Ryu et al., Chen et al., Martinez et al.).

Experimental studies (Table 1A) provide indispensable benchmarks, such as Han et al. reporting a 55% reduction in heat-exchange efficiency at 12° roll, or Simonini et al. directly resolving LN_2 interface velocities with PIV. However, these efforts are constrained by scale and environment: shaking tables cannot replicate long-duration microgravity, while surrogate fluids (e.g., LN_2 for LH_2) introduce thermal mismatches.

Numerical approaches (Table 1B) have become the dominant investigative tool, offering scalability and parametric flexibility. VOF-based CFD is the prevailing workhorse, effectively predicting interface evolution and boil-off trends, as demonstrated by Ryu et al., who reported a 66% increase in BOG at resonance. Yet validation studies (e.g., Baker & Hauser) reveal systematic bias: VOF often overpredicts condensation rates, particularly in regimes of violent free-surface breakup. This limitation stems from numerical diffusion in grid-based methods, a weakness that meshless frameworks such as SPH and MPS partially overcome. Freeman showed SPH reproduces slosh amplitudes within ±10% of experimental values, while Huang et al. demonstrated that MPS more accurately resolved pressure peaks in spherical LNG tanks than VOF. However, these gains in accuracy are offset by 3–5× higher computational demands, which restrict their current use to mid-TRL investigations.

Where structural survivability is at stake, coupled fluid–structure frameworks such as CEL and ALE prove indispensable. Ryali et al. captured both wall stresses exceeding 4 MPa and baffle deformation in LH_2 tanks, while Ma & Zhang employed ALE to reproduce rotary nonlinear sloshing with <8% deviation from experiment. These methods provide richer insight into tank integrity but remain setup-intensive and computationally expensive.

At the highest fidelity, DNS resolves all turbulent scales without modelling assumptions. Martinez et al. demonstrated that DNS predicted a ~40% rise in condensation and self-pressurization relative to quiescent cases. Yet with costs exceeding 100× VOF simulations, DNS remains confined to fundamental research rather than design cycles, serving primarily as a benchmark to validate reduced-order or CFD models.

Hybrid studies (Table 1C) provide perhaps the most balanced pathway forward. Li et al. combined SPH with bubble-point instability experiments to quantify damping, while Chen et al. paired VOF with surrogate-fluid experiments, confirming convection-driven BOG growth in LNG tanks. These hybrid approaches strengthen confidence in numerical predictions and offer a critical bridge between laboratory constraints and computational assumptions.

Collectively, these findings illustrate a clear stratification of methodological maturity: VOF-based CFD is entrenched as the high-TRL engineering standard, meshless and coupled approaches fill the mid-TRL niche for complex or nonlinear regimes, and DNS functions as a low TRL academic benchmark. Despite consensus on sloshing's capacity to accelerate BOG, critical disagreements persist over excitation-dependent cooling effects (Kang et al.) and the extent of VOF overprediction. The field's trajectory will therefore depend on greater comparative validation across methods and the integration of hybrid experimental-numerical studies to establish reliability beyond single-method conclusions.

7. Sloshing Mitigation Hardware (Baffles, PMDs, Active Control)

Managing the dynamic and often violent motion of cryogenic propellants, a phenomenon known as sloshing, remains one of the most formidable design challenges in aerospace engineering, with direct implications for vehicle safety and mission success. During critical manoeuvres such as engine ignition, stage separation, or orbital corrections, the vast liquid mass within propellant tanks can be set into motion. This sloshing triggers a cascade of complex fluid dynamics that threaten the mission on multiple fronts. The shifting centre of mass generates destabilizing torques capable of overwhelming the guidance, navigation, and control (GNC) system, while wave impacts against tank walls impose severe, localized loads that accelerate structural fatigue or even precipitate catastrophic failure. For cryogens like liquid hydrogen (LH_2) and liquid oxygen (LOX), vigorous liquid motion further enhances heat transfer from the walls, accelerating boil-off and compromising thermal management strategies.

The challenge is rooted in fluid nonlinearity. At low amplitudes, sloshing can be captured by linear theory, but in realistic flight conditions, the liquid often enters strongly nonlinear regimes marked by wave breaking, hydraulic jumps, and chaotic free-surface oscillations. These states magnify thermal and mechanical threats, rendering prediction and control far more difficult. To counter this, internal hardware, such as baffles and dampers, is traditionally installed to dissipate energy and stabilize the free surface. Yet, evidence shows their performance is highly sensitive to sloshing mode, excitation frequency, and tank geometry.

Recent research highlights both the strengths and limitations of existing suppression strategies, while also pointing to promising future directions. Incompressible SPH models have shown that damping screens in tuned liquid dampers (TLDs) can effectively enhance energy dissipation without excessive computational cost, providing a scalable option for large propellant tanks. At the same time, not all baffle configurations perform equally well: ring and horizontal baffles are most effective for damping symmetric low-order waves, whereas T-shaped baffles provide superior suppression of higher-order asymmetric modes. This mode dependence indicates that relying on a single baffle configuration across all operating conditions is insufficient. Other investigations have reinforced this conclusion, showing that even minor changes in perforation geometry, solidity ratio, or placement can significantly alter natural frequencies and nonlinear damping, underscoring the need for precise tailoring of internal structures.

Beyond structural designs, data-driven approaches are opening new pathways for predictive modelling and adaptive control. Machine learning–based frameworks have

been developed that successfully decompose nonlinear sloshing dynamics into linear and nonlinear components, enabling accurate prediction of chaotic transitions such as bursting and switching. Unlike conventional Fourier or wavelet methods, these models are computationally efficient and suitable for real-time implementation, pointing toward active or reconfigurable damping systems. Complementary Multiphysics simulations of LNG tanks further demonstrate that rigid baffles can suppress oscillations most effectively, whereas elastic baffles redistribute stresses to protect tank walls. Together, these findings suggest that material choice, geometry, and adaptability should be carefully linked to mission priorities whether the goal is maximum load reduction, extended fatigue life, or structural stress relief.

In summary, the literature shows that sloshing suppression is not a one-size-fits-all problem. Passive devices remain essential, but their effectiveness is mode- and configuration-dependent. Machine learning offers a promising complement by enabling fast, reduced-order characterization of nonlinear behaviour and by guiding the design of adaptive damping systems. For next-generation methane tanks where intermediate viscosity and strong gas–liquid coupling complicate dynamics the optimal path forward is a hybrid strategy: validated numerical modelling to explore design space, data-driven methods to identify dominant nonlinear regimes, and tailored damping structures (e.g., ring, T-shaped, perforated, or elastic baffles) selected according to operating mode. Such integration provides not only comparative insight but also a clear design solution for robust, mission-ready suppression of sloshing-induced vibrations. as seen in the Table 2 below.

Critical Synthesis of Sloshing Mitigation Hardware

The body of research on sloshing mitigation hardware reveals a clear technological progression, driven by a persistent tension between maximizing damping effectiveness and minimizing system-level penalties. As summarized in Table 2, a broad consensus confirms that passive baffles particularly fixed ring-type geometries are the most established and reliable means of disrupting bulk wave motion, dissipating kinetic energy, and suppressing slosh-induced pressure spikes in cryogenic tanks. The work of Zuo et al. and Seban et al. demonstrates how optimized baffle placement can significantly stabilize the cryogen free surface and mitigate pressure rise, reinforcing their status as a proven design solution. Yet this consensus is tempered by a critical counterpoint that defines the field: the inherent costs of structural integration. Studies by Lv et al. and Chung et al. highlight how conventional welded or bolted baffles form direct thermal bridges into the subcooled propellant, accelerating boil-off, while simultaneously introducing stress concentrations prone to cyclic fatigue. This trade-off robust slosh suppression at the expense of thermal and structural penalties remains the central conflict motivating continued innovation.

When examined across the Technology Readiness Level (TRL) scale, mitigation technologies can be stratified into distinct tiers. At the highest TRL, fixed, bottom-supported aluminium baffles remain the industry standard. As detailed by Bhavya et al. in reference to operational vehicles such as the PSLV, these designs are flight-proven, structurally well-characterized, and manufacturable on a scale. They represent the workhorse solution but fully embody the compromises of thermal leakage and long-term fatigue. Occupying the mid-TRL domain are dynamic passive systems, including floating and guided baffles explored by Gligor et al. and Abdullah et al. Validated through advanced numerical methods such as Smoothed Particle Hydrodynamics (SPH) and hybrid RANS–LES turbulence models, these devices adapt more effectively to low fill levels where fixed baffles lose efficiency. Their adaptability demonstrates meaningful damping benefits, but they introduce new challenges in long-term reliability, guidance mechanisms, and structural certification.

Table 2. Summary of Recent Studies on Baffle Effectiveness and Thermodynamics Behaviour.

Author(s)–Year [Ref.]	Tank/Fluid	Baffle Concept	Key Insight
Lv et al. [101,102],	Cylindrical/LH_2	Internal fixed baffles	Reduce pressure but introduce thermal bridging and joint stress (design trade-off).
Zuo et al. [103], Liu et al. [104].	Microgravity/LN_2; Cylindrical/LH_2	Optimized fixed baffles	Cut pressure rise; improved stratification under tuned excitation/fill.
Seban et al. [105], Momin et al. [106].	Cylindrical/semi-cryo; Rectangular/LOX	Ring baffles	Best performance near ~45% fill; ring geometry optimized for ISRO
Gligor et al.; Arif et al. [107,108].	Microgravity/LNG	Moving/floating baffles	Strong damping at low fill; floating baffles reduce wall pressure.
Bhavya et al. Im et al. [109,110].	PSLV/LH_2; Tanker	Bottom-supported multi-orifice aluminium baffles	Boil-off ~44% with multi-orifice designs; structurally practical.
Abdullah et al.; Liu et al. [111,112].	Membrane/LNG	Floating baffles with guides	Suppress waves; configurations validated in paired simulations
Varghese et al.; Furuichi et al. [113,114].	LN_2/LOX	Magnetic damping assist (hybrid expulsion)	Expulsion efficiency >90%; magnetic damping matches mechanical trends.
Rossetti et al.; Wu & He [115,116].	LNG fuel/Generic tank	Softer (compliant) baffles	Damping (≈85.3%) when baffle height $\geq$ fluid depth.
Chung et al. (2022) [117].	LH_2 cargo/Type-C	Ring baffles	Ring baffles can introduce fatigue risks over time (lifecycle consideration).
Xue et al., [118].	Rectangular, partially filled/water	Vertical baffles (several configs)	Vertical baffles suppress wall pressures; performance depends on configuration and frequency.
Xue & Lin, [119].	3-D prismatic/rectangular/ viscous liquid	Ring baffles	Ring baffles cut sloshing; effect depends on placement and width.
Xue et al., [120].	Cylindrical/LPG surrogate; harmonic + seismic input	Porous inner lining (porous "baffle" layer)	Porous layer dissipates energy, calming waves.
Zheng et al., [121].	Various tanks/fluids (review)	Survey of baffle strategies (vertical, ring, porous, etc.)	Comprehensive hydrodynamics review situating baffles within mitigation strategies; summarizes scaling, methods, and open gaps for design.

At the conceptual, low-TRL frontier are designs that aim to resolve the fundamental trade-off by decoupling damping performance from rigid structural elements. Examples include non-contact magnetic damping (Varghese et al.) and soft or flexible baffles that exploit fluid–structure interaction for enhanced dissipation (Rossetti et al.), with studies reporting up to an 85% increase in energy absorption compared with conventional configurations. These concepts are not yet flight-ready, but their ability to minimize thermal bridging while maintaining or exceeding damping performance makes them highly attractive for reusable and long-duration cryogenic stages.

More recent work extends this progression beyond purely structural interventions, toward adaptive and data-driven strategies. Parametric models such as NEWTANK (Xin Jin et al.) reveal that baffle effectiveness is mode-dependent: ring and horizontal baffles suppress symmetric low-order sloshing, while T-shaped baffles positioned at nodal locations are more effective for higher-order asymmetric modes. Complementary studies, including Faltinsen et al., show that even subtle changes in perforation geometry and solidity ratio significantly alter natural sloshing frequencies, highlighting the importance of precision-tailored damping structures. Numerical advances such as incompressible SPH frameworks (McNamara et al.) and SPH–FSI simulations (Chenxi Zhao et al.) now allow these relationships to be tested efficiently across nonlinear regimes, accounting for rigid versus elastic tank-wall behaviour. Importantly, elastic baffles are shown to redistribute

stress concentrations away from the tank walls, mitigating structural risk even if their free-surface suppression is less pronounced than rigid counterparts.

Finally, machine learning (ML) approaches represent a paradigm shift in slosh characterization and suppression. As demonstrated by Luo et al., ML frameworks can decompose complex nonlinear dynamics into linear and nonlinear components, capturing chaotic transitions such as bursting and switching with high fidelity. Unlike traditional frequency domain system identification, these models operate in real time and are computationally efficient, making them promising candidates for adaptive slosh control. When combined with reinforcement learning, they open the possibility of actively controlled or reconfigurable baffles that dynamically adjust their damping strategy in response to evolving sloshing conditions.

In conclusion, the technological evolution of slosh mitigation reflects a clear trajectory from robust but energy-inefficient fixed structures, through numerically validated adaptive passive systems, toward emerging contactless, flexible, and data-driven solutions that enhance energy dissipation and conversion efficiency while reducing thermal and structural penalties. For next-generation methane-fueled launch vehicles where intermediate viscosity, unique interfacial tension, and strong vapour–liquid coupling complicate oscillatory behaviour the future lies in hybrid energy-dissipative architectures. These combine validated passive configurations for baseline damping with machine-learning-assisted adaptive controllers capable of modulating slosh energy in nonlinear, mode-specific regimes. Such integrated frameworks are not only expected to suppress dynamic loads, but also to stabilize energy exchange between mechanical motion and thermal processes, minimizing boil-off losses and ensuring sustained structural health across long-duration and reusable cryogenic missions.

8. Representative Rocket Engines and Launch Vehicles Using Cryogenic Propellants

Cryogenic propellants liquid hydrogen (LH_2), liquid oxygen (LOX), and increasingly liquid methane (CH_4) form the backbone of modern launch-vehicle propulsion. Their low temperature, low viscosity, and high vapour pressure make sloshing particularly severe, inducing dynamic loads, pressure fluctuations, and feed-system instabilities; historical vehicles such as the Soviet R-7 (Soyuz) family and the heavy-lift Energia program provide early practical examples of how cryogenic tanks and feedlines must be managed in flight. Documented flight anomalies and structural failures across programs highlight the criticality of sloshing control in cryogenic tanks. While mitigation measures such as baffles, diaphragms, damping rings, and tuned fluid–structure interactions are widely applied, the growing adoption of methane introduces new considerations. Unlike LH_2, methane offers higher density, simpler handling, reduced leakage losses, and the possibility of in situ resource utilization (ISRU) on Mars. Compared to LOX, it provides cleaner combustion products and greater reusability, making it the propellant of choice in next-generation engines such as SpaceX's Raptor and Blue Origin's BE-4. These operational advantages, however, are coupled with distinct sloshing dynamics that demand tailored analysis. Jeon et al. showed that sloshing motion in cryogenic methane tanks can increase boil-off gas (BOG) generation by up to 289%, with resonance at short sloshing periods amplifying vaporization far beyond static conditions. This differs from hydrogen, where extremely low viscosity drives violent free-surface instabilities, and from oxygen, where sloshing is less strongly tied to thermodynamic effects. Jin et al. demonstrated that viscosity modifies resonance behaviour and induces phase lag between pressure response and excitation. Methane, with viscosity higher than LH_2 yet lower than storable propellants, occupies a transitional regime where damping is significant, but instability remains critical.

Numerical evidence reinforces this distinction. Brodnick (NASA) found that low liquid-to-gas density ratios in methane systems cause gas inertia to reduce natural frequency, shift effective slosh mass, and elevate damping effects negligible in LOX tanks but profound in methane and LH_2. Similarly, Baker & Hauser reproduced historical K-site methane slosh-drain tests, showing that accurate predictions of pressurization and stratification require turbulence and interfacial-damping models absent in classical LH_2/LOX approaches. For mitigation, Strahan's Morpheus program confirmed that ring baffles tailored for methane/LOX tanks can effectively suppress slosh-control coupling, while Yang & Williams validated multiphase CFD simulations of methane sloshing and draining against NASA experimental data, ensuring reliable performance prediction for operational scenarios. Taken together, these studies show that methane's unique balance of performance, storability, and resource accessibility explains its growing preference in modern propulsion but also highlight that its sloshing behaviour cannot be extrapolated directly from hydrogen or oxygen. Instead, methane requires dedicated models and mitigation strategies that account for its intermediate viscosity, distinct interfacial tension, and strong coupling with gas dynamics [122]. These dual operational advantages paired with complex sloshing physics explain both the attraction to methane as a propellant and the necessity of deeper research into its dynamic characteristics.

Table 3 summarizes representative cryogenic rocket engines and stages. It lists propellant pairs, tank volumes, recorded sloshing issues, and implemented suppression features. This overview illustrates the range of sloshing phenomena encountered and the tailored solutions required in cryogenic propulsion design.

Table 3. Summary of Representative Cryogenic Rocket Engines and Stages.

Engine/Stage	Propellant Combination	Oxidizer Tank Volume (m^3)	Fuel Tank Volume (m^3)	Known Sloshing Issues	Sloshing Mitigation Features
Saturn V (S-IC stage)	LOX/RP-1	120	810	LOX sloshing induced feedline cavitation	Anti-slosh baffles in the LOX tank
Saturn V (S-II stage)	LOX/LH_2	328	946	LH_2 sloshing + pogo coupling (dynamic instability)	Slosh baffles+ accumulators in the feed system
Space Shuttle SSME	LOX/LH_2	550 (LOX ET)	1460 (LH_2 ET)	LH_2 low damping ratio, pogo oscillations	Baffles, surge suppressors, helium prepress
Ariane 5 Vulcain 2	LOX/LH_2	170	400	LOX sloshing affecting feed pressure stability	Swash bulkheads, baffles in the LOX tank
Delta IV RS-68	LOX/LH_2	250	550	LH_2 sloshing influencing feedline stability	LOX anti-vortex devices, baffles
Falcon 9 Merlin	LOX/RP-1	Classified	Classified	Limited data: Slosh likely controlled	standard baffles, pressurization control
H-II LE-7A	LOX/LH_2	200	600	LH_2 sloshing impacting the turbopump inlet flow	Anti-slosh rings, bulkheads
Atlas V RD-180 + Centaur	LOX/RP-1 (core), LOX/LH_2 (upper)	190 (LOX core), ~45 (LH_2 Centaur)	95 (RP-1 core), ~96 (LH_2 Centaur)	Centaur upper stage LH_2 slosh critical for attitude control	Slosh baffles and tuned mass dampers
N1 Rocket (NK-33 engine)	LOX/RP-1	Classified	Classified	Soviet-era, limited public data	Baffles presumed standard
GSLV Mk-III CE-20	LOX/LH_2	120	200	Sloshing analysis conducted-in design phase	Baffles, anti-slosh rings
New Glenn BE-4	LOX/LNG (methane)	Classified	Classified	Sloshing mitigation details undisclosed	Similar to LOX/LH_2 systems
R-7 (Soyuz)	LOX/RP-1	Varies by variant; multi-tank configuration (core + boosters)	Varies by variant	Coupled sloshing between core and strap-on boosters; low frequency modes affecting feed stability	Perforated baffles, anti-vortex devices, baffled inter-tank ducts.
Energia	LOX/LH_2	Large cryogenic tanks (exact data limited)	Large cryogenic tanks (exact data limited)	High propellant mass fraction caused low-frequency oscillations; strong fluid–structure interaction during testing	Internal Baffle Webs, baffled LH_2 tanks, feedline dampers

8.1. Critical Synthesis of Representative Cryogenic Rocket Engines and Stages

The historical data from operational launch vehicles reveals a powerful consensus on the primary methodology for slosh mitigation: the universal adoption of passive mechanical hardware. Across decades of vehicle design, from the Saturn V to the modern

GSLV, a clear reliance on baffles, anti-slosh rings, and swash bulkheads demonstrates this single, dominant approach. This consensus is particularly strong for managing low-density, low-damping cryogens like LH_2, which is consistently identified as a source of instability. However, while the use of baffles is a constant, a key point of disagreement or more accurately, a divergence in approach emerges in the sophistication required for the mitigation strategy. For most core stages, simple baffles are deemed sufficient. In contrast, for precision-critical applications like upper stages, a more advanced methodology is required. This is best illustrated by the Atlas V Centaur, which augments traditional baffles with tuned mass dampers to ensure precise attitude control, a clear departure from the purely passive systems on most other vehicles.

In terms of technological maturity, passive ring and swash baffles represent a quintessential high TRL solution, with over 60 years of flight heritage making them the default, most reliable engineering choice. Similarly, secondary systems like feedline accumulators and surge suppressors (seen on Saturn and Shuttle) are also mature, high-TRL technologies, though they are tailored to address the specific problem of pogo oscillations rather than general slosh. The use of tuned mass dampers, while a mature technology in principle, represents a more advanced and specialized high TRL application within this context. The limited public data on modern vehicles like Falcon 9 and the future New Glenn suggests a continued reliance on these proven, high TRL methods, though the introduction of new propellants like LNG may eventually necessitate new or refined mitigation strategies.

8.2. Comparative Sloshing Characteristics of Cryogenic Propellants

Cryogenic propellants liquid hydrogen (LH_2), liquid oxygen (LOX), and the increasingly prominent liquid methane (CH_4) form the foundation of current and next-generation propulsion architectures. Their low viscosity, high volatility, and temperature sensitivity make them inherently prone to sloshing-induced pressure fluctuations, structural fatigue, and dynamic instabilities. While LH_2 and LOX have been extensively studied over decades of flight heritage from Saturn V to the Space Shuttle—methane has emerged as a transitional propellant bridging classical and advanced cryogenic regimes.

Methane's intermediate viscosity and density place it between hydrogen and oxygen, producing unique sloshing signatures characterized by measurable damping yet persistent instability. Experimental and computational investigations reveal that methane sloshing enhances boil-off gas (BOG) generation by nearly 300% under resonant excitation, coupling mechanical oscillations directly to phase-change heat transfer. Unlike hydrogen, where extreme fluid mobility and low surface tension promote high-frequency chaotic wave motion, or oxygen, where sloshing remains largely inertial and weakly coupled to thermodynamic behaviour, methane's moderate viscous damping and strong gas–liquid coupling cause energy dissipation to dominate its dynamic response.

These thermo-viscous interactions define a distinct energy-conversion pathway: part of the sloshing kinetic energy is continuously dissipated as heat through vaporization and interfacial shear, accelerating boil-off but simultaneously providing self-damping that moderates structural loads. Numerical models confirm that methane's low liquid-to-gas density ratio alters natural frequency and shifts the effective slosh mass distribution, producing frequency softening and non-linear attenuation behaviour not captured by LH_2/LOX analogues. Consequently, classical mitigation hardware—such as ring baffles or swash bulkheads—remains effective for hydrogen and oxygen but requires re-optimization for methane's coupled thermodynamic regime.

In practice, modern engines such as SpaceX's Raptor and Blue Origin's BE-4 exemplify this evolution. Their CH_4/LOX configurations integrate high-TRL passive damping elements with active venting and predictive control, embodying a new hybrid architecture

that merges structural and thermodynamic management. Methane's clean combustion and in situ resource utilization (ISRU) potential for Mars missions further reinforces its growing strategic value. Yet its sloshing energy dissipation behaviour—lying between hydrogen's volatility and oxygen's stability demands refined multi-physics models capable of resolving nonlinear phase coupling, interfacial damping, and structural feedback.

In summary, methane's emergence represents both an engineering opportunity and a modelling challenge. Its unique position in the cryogenic spectrum offers operational advantages in storability, reusability, and ISRU compatibility but necessitates an updated theoretical and experimental framework for sloshing-induced energy dissipation. The path forward involves extending validated LH_2/LOX methodologies with methane-specific damping correlations, adaptive baffle optimization, and integrated thermo-fluid control critical steps toward achieving stable, energy-efficient propulsion for the next era of reusable and deep-space vehicles.

8.3. Future Direction and Application of AI and Digital Twins in Sloshing Management

Artificial intelligence (AI) has become an increasingly powerful framework for modelling and mitigating liquid sloshing, offering predictive accuracy and computational efficiency beyond classical analytical or CFD-based approaches. Traditional models, though physically interpretable, often struggle to capture nonlinear free-surface dynamics, vapour–liquid interactions, and transient coupling in cryogenic environments. In contrast, AI can approximate these behaviours directly from data, allowing for rapid evaluation once trained.

A hybrid Particle Swarm Optimization–Radial Basis Function Neural Network (PSO–RBFNN) model successfully predicted sloshing wave height and pressure under seismic excitation, identifying key controlling parameters such as PGV, PGA/PGV, and fill ratio [123]. Despite its accuracy, performance degraded when training data lacked variability—reflecting the inherent dependence of conventional AI on large, diverse datasets. To address this, a GAN-based data augmentation with Bayesian-Optimized XGBoost (BO-XGBoost) was proposed, enabling synthetic dataset generation while maintaining interpretability through SHAP analysis [124]. This improved generalization but underscored the reviewer's observation that AI still requires costly high-fidelity validation data to achieve engineering reliability.

Subsequent studies strengthened the physical basis for training through experimental and numerical datasets on elastic and annular tanks [125,126] and nonlinear fluid–shell coupling [127]. These works quantified how geometry, damping, and wall compliance affect natural frequencies and modal amplitudes—parameters now embedded as features in modern machine learning models. Integration with coupled CFD–AI frameworks further clarified the damping role of internal baffles and excitation spectra on sloshing loads [128–130].

Recognizing that data-driven models alone cannot guarantee physical consistency, recent research has shifted toward Physics-Informed Neural Networks (PINNs)—a hybrid class of models that embed governing fluid and structural equations (e.g., Navier–Stokes, mass continuity, and wall deformation) directly into the training loss function. This allows PINNs to learn continuous solutions constrained by conservation laws rather than discrete data alone [131,132]. In sloshing applications, PINNs have been used to reconstruct velocity and pressure fields from sparse sensors, predict free-surface evolution under arbitrary excitation, and quantify interfacial damping in partially filled tanks without requiring dense CFD datasets. This fundamentally reduces data dependence while improving extrapolation to untested boundary conditions—precisely addressing the reviewer's concern about data scarcity and training cost.

Comparative studies confirmed that Artificial Neural Networks (ANNs) outperform Genetic Algorithms (GAs) in capturing free-surface displacement and wall force responses,

achieving <7% average error once trained [133]. However, even these models benefit when informed by physically consistent constraints. Recent works using SPH-based datasets for Multilayer Feed-Forward and Recurrent Neural Networks have shown similar accuracy gains when physical regularization terms are introduced [134]. Moreover, image-based deep learning (ResNet) methods reconstructing wall pressure fields from free-surface images demonstrated that integrating physical priors—such as Froude similarity or frequency ratios—enhances transferability between tanks of different geometries [135].

These advances have converged toward real-time implementations through digital twins, where AI-predicted states are dynamically updated using sensor feedback and on-board computation [136]. Such frameworks allow active slosh suppression by adjusting venting sequences, baffle stiffness, or thrust vector alignment in flight.

Parallel progress in cryogenic research reveals that methane-based propellants exhibit sloshing dynamics distinct from hydrogen or oxygen due to intermediate viscosity, surface tension, and gas coupling effects [137–139]. For accurate modelling, nonlinear FSI–fatigue coupling must be considered in Composite Overwrapped Pressure Vessels (COPVs) under repeated thermal–mechanical cycling [140]. Coupled SPH–FSI simulations confirm that rigid baffles best suppress wave amplitude, whereas elastic baffles redistribute structural stresses, enhancing long-term stability [141,142]. recent developments reflect a clear transition from conventional data-intensive AI toward physics-informed and hybrid intelligence frameworks. These emerging models aim to bridge the gap between data efficiency and physical fidelity, offering faster, more interpretable, and more generalizable predictions. By embedding governing equations and conservation laws directly into the learning process, such approaches reduce reliance on vast experimental or computational datasets while improving extrapolation to new operating conditions. Integrating these models within digital-twin environments will enable real-time monitoring, adaptive control, and automated decision-making for sloshing suppression during launch or in-orbit operations.

Looking ahead, advancing this field requires systematic benchmarking between data-driven and physics-informed methods, development of shared cryogenic databases for model training and validation, and exploration of transfer learning to extend applicability across varying gravity and thermal regimes. The convergence of AI, experimental sensing, and Multiphysics modelling will ultimately define the next generation of cryogenic propellant management—one that balances accuracy, efficiency, and reliability while addressing the cost and complexity of large-scale AI training identified by the reviewer.

8.4. Literature Search Strategy

To construct a comprehensive and authoritative review, we implemented a rigorous literature search protocol designed to capture the full spectrum of cryogenic sloshing research. The search spanned Scopus, Web of Science, and the NASA Technical Reports Server (NTRS), ensuring balanced coverage of both peer-reviewed academic studies and applied aerospace engineering reports. The temporal scope was set to the modern innovation period of 2000–2025, intentionally augmented with seminal pre-2000 works (e.g., Dodge, NASA SP-106) to provide historical continuity. The search strategy employed a layered approach. Broad terms such as “cryogenic sloshing” and “propellant sloshing” were first deployed to establish comprehensive coverage. These were progressively refined to highly specific technical terms including “composite tank FSI,” “cryogenic CFD,” “magnetic damping,” “sloshing baffles,” and “microgravity propellant dynamics.” Boolean operators (AND, OR) were used to ensure relevant intersections across fluid–structure interaction, thermodynamic coupling, and slosh-control technologies.

In total, 520 records were retrieved across all databases. After removal of 72 duplicates, 448 unique studies were screened by title and abstract. Of these, 273 were excluded for lack

of aerospace or cryogenic relevance (e.g., purely seismic or civil water-tank studies). The remaining 175 full texts were assessed for eligibility, leading to the exclusion of 50 works that did not meet methodological or contextual thresholds. The final synthesis incorporated 138 references, comprising peer-reviewed journal articles, conference proceedings, and NASA technical reports. From each included work, structured data were extracted to enable consistent comparison. Extracted variables included bibliographic details (authors, year, DOI/report number), tank geometry and boundary conditions, cryogen type (LH_2, LOX, LNG surrogate), gravity regime (1-g, reduced-g, or microgravity), methodological approach (experimental, analytical, or computational), excitation conditions, and reported outcomes such as natural frequencies, damping ratios, heat transfer, or stability margins. As elaborated in Table 4.

Table 4. Summary of Literature Search Protocol.

Component	Description
Databases searched	Scopus, Web of Science, NASA Technical Reports Server (NTRS)
Timeframe	2000–2025 (modern innovation period) + seminal pre-2000 works
Search strategy	Layered queries: broad terms ('cryogenic sloshing') → specific terms ('composite tank FSI,' 'cryogenic CFD,' 'magnetic damping,' 'sloshing baffles') with Boolean operators
Records retrieved	520
Duplicates removed	72
Screened (title/abstract)	448
Excluded (non-cryogenic/non-aerospace)	273
Full texts assessed	175
Excluded at full-text stage	50
Final references included	138
Inclusion criteria	Peer-reviewed journal articles, conference proceedings, and NASA technical reports directly addressing cryogenic sloshing in aerospace
Exclusion criteria	Non-peer-reviewed (except NASA reports), civil-only sloshing (unless transferable), duplicates
Data extracted	Bibliographic info, tank geometry, fluid type, gravity regime, methodology, excitation, outcomes (natural frequencies, damping, heat transfer, stability)

9. Conclusions

This review has examined the sloshing behaviour of cryogenic propellants through experimental, numerical, and analytical methods, reframed in terms of the energy pathways that drive inefficiency and dissipation. Experimental campaigns have evolved from early drop-tower and parabolic-flight tests to orbital demonstrations with high-fidelity diagnostics, but they remain constrained by short time windows and scale effects that obscure the thermally coupled mechanisms where energy is lost through turbulence, wave breaking, and boil-off (Liu et al.). Numerical approaches based on VOF and SPH CFD have made significant progress in resolving free-surface motion, pressure oscillations, and thermal stratification (Xue et al., Zheng et al.), yet their accuracy remains limited when turbulence closures or constant-property assumptions mask the true dissipation channels. Analytical and semi-empirical models (Jin et al., Liu et al.) continue to provide first-order estimates of slosh-induced forces and energy transfer, but their generalization across varying geometries, fill fractions, and excitation modes is narrow. More recently, AI-assisted frameworks have shown promise in capturing dissipative dynamics more efficiently, offering predictive surrogates that balance accuracy and interpretability for sloshing under variable gravity and seismic excitation.

Limitations in current techniques can be understood as blind spots in quantifying energy losses. Earth-based experiments are time-limited and scale-restricted, underestimating cumulative dissipation under long-duration microgravity. Parabolic flights and drop towers yield only seconds of usable data, while orbital experiments remain rare and prohibitively expensive (Storey). Numerical simulations, though powerful, are computationally costly and risk underpredicting dissipation when property variations, phase-change kinetics, or fluid–structure interactions are significant. Analytical models, while efficient, often linearize the problem and neglect boundary-layer effects or vapour generation, overlooking key energy sinks in cryogenic systems. Collectively, these limitations emphasize the need for integrated strategies that not only capture liquid motion but also quantify how sloshing dissipates stored cryogenic enthalpy into turbulence, boil-off, and unnecessary control work.

Looking ahead, several energy-focused directions are clear. Long-duration flight experiments are essential to benchmark energy dissipation mechanisms under sustained microgravity and gravity transitions. Multiphysics numerical models should aim to unify turbulence, capillarity, phase change, and structural coupling, with validation against measured dissipation rates rather than only free-surface profiles. AI-driven surrogates and digital twin frameworks (Jin et al., Liu et al.) offer promise in predicting and managing dissipative dynamics in real time, especially when linked with active damping and feedback systems to minimize corrective energy expenditure. For aerospace engineering, the stakes are high: managing energy dissipation in cryogenic storage and transfer is central to extending loiter times, reducing boil-off, and preserving propulsive efficiency cornerstones for the viability of next-generation launchers, orbital depots, and deep-space missions.

Author Contributions: Conceptualization, A.J.E.; Methodology, A.J.E. and X.Z.; Software, A.J.E.; Validation, A.J.E., X.Z. and M.P.; Formal Analysis, A.J.E.; Investigation, A.J.E.; Resources, X.Z.; Data Curation, A.J.E.; Writing—Original Draft Preparation, A.J.E.; Writing—Review and Editing, X.Z., M.P., T.S., J.E. and C.M.T.T.; Visualization, A.J.E.; Supervision, X.Z., M.P., T.S., J.E. and C.M.T.T.; Project Administration, X.Z.; Funding Acquisition, X.Z. All authors have read and agreed to the published version of the manuscript.

Funding: This research was funded by Australia–UK Renewable Hydrogen Innovation Partnerships, grant number AUKRH000031, Shock, Vibration, and Sloshing Behaviour of Type V Hydrogen Cryogenic Tanks. The APC was funded by Australia–UK Renewable Hydrogen Innovation Partnerships.

Data Availability Statement: The original contributions presented in the study are included in the article, further inquiries can be directed to the corresponding author/s.

Conflicts of Interest: The authors declare no conflict of interest.

Nomenclature

Abbreviations and Acronyms

NASA	National Aeronautics and Space Administration
GRC	Glenn Research Centre
CFM	Cryogenic Fluid Management
CONE	Cryogenic Orbital Nitrogen Experiment
CFME	Cryogenic Fluid Management Experiment
COLD-SAT	Cryogenic On-Orbit Liquid Depot Storage, Acquisition & Transfer Satellite
CPST	Cryogenic Propellant Storage and Transfer Demonstration Mission
PMD	Propellant Management Devices
ZBO	Zero Boil-Off
VCS	Vapour Cooling System

TVS	Thermodynamic Vent System
FO	Filling Operations
PTCD	Propellant Chill-Down
TO	Transfer Operations
HP/AP	Heterogeneous/Autogenous Pressurization
ISS	International Space Station
COPV	Composite Overwrapped Pressure Vessel
LAD	Liquid Acquisition Device
SSE	SPHERES-Slosh Experiment
SPHERES	Synchronized Position Hold Engage and Reorient Experimental Satellites
NT-SPARGE	Non-Isothermal Sloshing Parabolic Flight Experiment
FLUIDICS	ESA/ISS Sloshing Experiment
StELIUM	UNOOSA DropTES Ferrofluid Sloshing Experiment
CFD	Computational Fluid Dynamics
FSI	Fluid–Structure Interaction
VOF	Volume of Fluid
SPH	Smoothed Particle Hydrodynamics
MPS	Moving Particle Semi-implicit
CEL	Coupled Eulerian–Lagrangian
DNS	Direct Numerical Simulation
RANS	Reynolds-Averaged Navier–Stokes
FVM	Finite Volume Method
LBM	Lattice Boltzmann Method
CLSVOF	Coupled Level Set/Volume of Fluid
UDF	User-Defined Function
AIAD	Algebraic Interfacial Area Density
TRL	Technology Readiness Level
BOG	Boil-Off Gas
Cryogenic Fluids	
LH_2	Liquid Hydrogen
LOX	Liquid Oxygen
LCH_4	Liquid Methane
LF_2	Liquid Fluorine
LN_2	Liquid Nitrogen
LAr	Liquid Argon
SLH_2	Slush Hydrogen
Symbols and Variables	
ρ	Density
V	Mean velocity vector
p	Pressure
μ	Dynamic viscosity
μt	Eddy viscosity
g	Gravitational acceleration
Fvol	Volume force
E	Energy term
λ	Thermal conductivity/empirical constant
Sm, Sh	Mass source term, Energy source term
r, R	Tank radius (cylindrical/spherical)
h	Liquid height
ξm	Root of eigenvalue equation
ωm	Angular frequency (cylinder)
fm	Natural frequency (Hz)
ωn	Angular frequency (sphere)

ω0	Excitation frequency
X0	Excitation amplitude
K1, K2	Empirical constants
ΔQabs	Net absorbed heat
Qr	Radiative heat transfer
Qsc	Solid conduction
Qgc	Gaseous conduction
ΔQs	Heat stored in vessel structure
As, Ah	Inner/outer surface areas
Th, Ts	Outer/inner surface temperatures
εs, εh	Emissivities
σ	Stefan–Boltzmann constant
k	Thermal conductivity
l	Thickness
ΔT	Temperature difference
PG	Gas pressure
M	Molecular mass
TG	Gas temperature
W	Mass of the vessel
Cp	Specific heat
ΔTs	Wall temperature change
Pbo	Percentage boil-off
hv	Latent heat of vaporization
V	Volume of cryogen
ρsl	Initial density
Q	Heat input
ΔH	Enthalpy change
v	Specific volume
ΔP	Pressure change

References

1. Xu, W.; Li, Q.; Huang, M. Design and analysis of liquid hydrogen storage tank for high-altitude long-endurance remotely-operated aircraft. *Int. J. Hydrogen Energy* **2015**, *40*, 16578–16586. [CrossRef]
2. Svensson, F.; Hasselrot, A.; Moldanova, J. Reduced environmental impact by lowered cruise altitude for liquid hydrogen-fuelled aircraft. *Aerosp. Sci. Technol.* **2004**, *8*, 307–317. [CrossRef]
3. Tiwari, S.; Pekris, M.J.; Doherty, J.J. A review of liquid hydrogen aircraft and propulsion technologies. *Int. J. Hydrogen Energy* **2024**, *57*, 1174–1196. [CrossRef]
4. Xie, F.S.; Xia, S.Q.; Zhu, Y.H.; Ma, Y.; Li, Y.Z.; Xiong, L.Y.; Lu, C.A. Visual experimental study of slush hydrogen production by freezing-melting method. *Cryogenics* **2023**, *131*, 103663. [CrossRef]
5. Meyer, M.L.; Motil, S.M.; Ginty, C.A.; Melis, M.E. Cryogenic propellant storage and transfer technology demonstration for long-duration in-space missions (NASA Technical Report). In Proceedings of the Space Propulsion 2012, Bordeaux, France, 7–10 May 2012; NASA Technical Reports Server: Cleveland, OH, USA, 2012.
6. Omsik, T.M. Recent advances and applications in cryogenic propellant densification technology (NASA Technical Memorandum 20994). In Proceedings of the Intersociety Cryogenic, Atlanta, GA, USA, 5–9 March 2000; NASA: Greenbelt, MD, USA, 2000.
7. Motil, S.M.; Meyer, M.L.; Tucker, S.P. Cryogenic fluid management technologies for advanced green propulsion systems (NASA Technical Report TM-2007-214810). In Proceedings of the 45th AIAA Aerospace Sciences Meeting and Exhibit, Reno, NV, USA, 8–11 January 2007; NASA: Greenbelt, MD, USA, 2007.
8. He, M.; Lv, C.; Gong, L.; Wu, J.; Zhu, W.; Zhang, Y.; Zhang, M.; Sun, W.; Sha, L. The design and optimization of a cryogenic compressed hydrogen refueling process. *Int. J. Hydrogen Energy* **2021**, *46*, 29391–29399. [CrossRef]
9. Abramson, H.N. *The Dynamic Behavior of Liquids in Moving Containers, with Applications to Space Vehicle Technology (NASA Special Publication SP-106)*; NASA: Greenbelt, MD, USA, 1996.
10. Simonini, A.; Dreyer, M.; Urbano, A.; Sanfedino, F.; Himeno, T.; Behruzi, P.; Avila, M.; Pinho, J.; Peveroni, L.; Gouriet, J.B. Cryogenic propellant management in space: Open challenges and perspectives. *Npj Microgravity* **2024**, *10*, 34. [CrossRef]

11. Berglund, M.D.; Bassett, C.E.; Kelso, J.M.; Mishic, J.; Schrage, D. The Boeing Delta IV launch vehicle—Pulse-settling approach for second-stage hydrogen propellant management. *Acta Astronaut.* **2007**, *61*, 416–424. [CrossRef]
12. ANSYS Inc. *ANSYS Fluent Theory Guide 15317*; ANSYS Inc.: Canonsburg, PA, USA, 2011.
13. Dodge, F.T. *The New "Dynamic Behavior of Liquids in Moving Containers"*; Southwest Research Institute: San Antonio, TX, USA, 2000.
14. Ibrahim, R.A. *Liquid Sloshing Dynamics: Theory and Applications*; Cambridge University Press: Cambridge, UK, 2005.
15. Miller, J.H.; El-Awady, J.M.; Kolb, C.E. Experimental results of hydrogen slosh in a 62 cubic foot (1750 L) tank (AIAA Paper No. 98-3521). In Proceedings of the 34th Joint Propulsion Conference and Exhibit, Cleveland, OH, USA, 13–15 July 1998; American Institute of Aeronautics and Astronautics: Washington, DC, USA, 1998.
16. Knoll, R.H.; Nunamaker, R.R.; Smolak, G.R. *Weightlessness Experiments with Liquid Hydrogen in Aerobee Sounding Rockets, Uniform Radiant Heat Addition—Flight 1 (NASA Technical Memorandum TM X-484)*; NASA: Greenbelt, MD, USA, 1963.
17. Li, J.C.; Lin, H.; Li, K.; Wu, B.; Zhu, Q. Liquid sloshing in partially filled capsule storage tank undergoing gravity reduction to low/micro-gravity condition. *Microgravity Sci. Technol.* **2020**, *32*, 587–596. [CrossRef]
18. Hou, C.; Yu, Y.; Liu, X.; Ding, J.; Cui, Z. Effects of longitudinal excitation on liquid hydrogen sloshing in spacecraft storage tanks under microgravity conditions. *Int. J. Hydrogen Energy* **2024**, *51 Pt D*, 765–780. [CrossRef]
19. Jiang, Y.; Yu, Y.; Wang, Z.; Zhang, S.; Cao, J. CFD simulation of heat transfer and phase change characteristics of the cryogenic liquid hydrogen tank under microgravity conditions. *Int. J. Hydrogen Energy* **2023**, *48*, 7026–7037. [CrossRef]
20. Wang, J.; Li, Y.; Wang, L.; Xia, S.; Ren, J.; Mao, H.; Xu, Y. Numerical investigation on subcooled pool film boiling of liquid hydrogen in different gravities. *Int. J. Hydrogen Energy* **2021**, *46*, 2646–2657. [CrossRef]
21. Hartwig, J.; Chato, D.; McQuillen, J. Screen channel LAD bubble point tests in liquid hydrogen. *Int. J. Hydrogen Energy* **2014**, *39*, 853–861. [CrossRef]
22. Liu, Z.; Li, Y.; Zhou, G. Study on thermal stratification in liquid hydrogen tank under different gravity levels. *Int. J. Hydrogen Energy* **2018**, *43*, 9369–9378. [CrossRef]
23. Kong, W.; Tian, Q. Dynamics of fluid-filled space multibody systems considering the microgravity effects. *Mech. Mach. Theory* **2020**, *148*, 103809. [CrossRef]
24. Nadeem, S.; Bosca, P.; Stramenga, M.; Casella, J.; Coppens, J.; Henriques, J.; Wynn, G.; Hamed, M. An experimental investigation of slat-screens to mitigate fluid sloshing in microgravity. *J. Space Saf. Eng.* **2022**, *9*, 319–327. [CrossRef]
25. Romero-Calvo, Á.; García-Salcedo, A.J.; Garrone, F.; Rivoalen, I.; Cano-Gómez, G.; Castro-Hernández, E.; Herrada Gutiérrez, M.Á.; Maggi, F. StELIUM: A student experiment to investigate the sloshing of magnetic liquids in microgravity. *Acta Astronaut.* **2020**, *173*, 344–355. [CrossRef]
26. Dalmon, A.; Lepilliez, M.; Tanguy, S.; Garnier, V. Comparison between the FLUIDICS experiment and direct numerical simulations of fluid sloshing in spherical tanks under microgravity conditions. *Microgravity Sci. Technol.* **2019**, *31*, 123–138. [CrossRef]
27. Bašic, J.; Blagojevic, B.; Bašic, M.; Klarin, B. Lagrangian differencing dynamics for microgravity sloshing. In Proceedings of the 2021 6th International Conference on Smart and Sustainable Technologies, Split & Bol, Croatia, 8–11 September 2021.
28. Ma, B.; Yue, B. Arbitrary Lagrangian–Eulerian finite element method for liquid sloshing with contact angle hysteresis in microgravity. *Adv. Space Res.* **2025**, *75*, 1585–1596. [CrossRef]
29. Da Fonseca, I.M.; Bainum, P.M. CSI due to sloshing motion on LEO LSS. *Adv. Astronaut. Sci.* **2012**, *145*, 1073–1108.
30. Sah, R.; Srivastava, R.; Lima, R.; Vatsal, V.; Das, K. Numerical modeling of liquid propellant mass transfer with sloshing during on-orbit refueling. In Proceedings of the 2024 IEEE Aerospace Conference, Big Sky, MT, USA, 2–9 March 2024; IEEE: New York, NY, USA, 2024; pp. 1–14. [CrossRef]
31. Orr, J.S. Modeling and simulation of rotary sloshing in launch vehicles. In Proceedings of the 31st AAS/AIAA Space Flight Mechanics Meeting, Charlotte, Carolina, 1–4 February 2021; American Astronautical Society: Springfield, VA, USA, 2021.
32. Monteiro, F.; Marques, P.A.; Simonini, A.; Carbonnelle, L.; Méndez, M.A. Experimental characterization of non-isothermal sloshing in microgravity. *Exp. Therm. Fluid Sci.* **2025**, *166*, 111473. [CrossRef]
33. Storey, J.M. *Experiments and Simulations of Liquid Mass Gauging and Slosh Dynamics in Microgravity (Doctoral Dissertation)*; Florida Institute of Technology: Melbourne, FL, USA, 2023.
34. American Astronautical Society. In Proceedings of the AAS3rd International Space Station Research Development Conference, Seattle, DC, USA, 30 June 2014; American Astronautical Society: Chicago, IL, USA, 2014.
35. Romero-Calvo, Á.; Akay, Ö.; Schaub, H.; Schaub, H.; Brinkert, K. Magnetic phase separation in microgravity. *Npj Microgravity* **2022**, *8*, 32. [CrossRef]
36. Carollo, R.A.; Aveline, D.C.; Rhyno, B.; Vishveshwara, S.; Lannert, C.; Murphree, J.D.; Elliott, E.R.; Williams, J.R.; Thompson, R.J.; Lundblad, N. Observation of ultracold atomic bubbles in orbital microgravity. *Nature* **2022**, *606*, 281–286. [CrossRef]
37. Wang, Z.; Mérida, W. Thermal performance of cylindrical and spherical liquid hydrogen tanks. *Int. J. Hydrogen Energy* **2024**, *53*, 667–683. [CrossRef]

38. Liu, Y.; Hao, Y.; Li, F.; Shen, J.; Xing, Z.; Zhou, H. Simulation study on the influencing factors of thermal conductivity of large-volume vehicle-mounted liquid hydrogen bottles under different filling rates. *Int. J. Hydrogen Energy* **2024**, *69*, 804–816. [CrossRef]
39. Liu, Z.; Li, Y.; Lei, G.; Xia, S.; Li, C. Experimental study on refrigeration performance and fluid thermal stratification of thermodynamic vent. *Int. J. Refrig.* **2018**, *88*, 496–505. [CrossRef]
40. Liu, Z.; Feng, Y.; Lei, G.; Li, Y. Fluid thermal stratification in a non-isothermal liquid hydrogen tank under sloshing excitation. *Int. J. Hydrogen Energy* **2018**, *43*, 22622–22635. [CrossRef]
41. Zuo, Z.; Jiang, W.; Qin, X.; Huang, Y. Numerical investigation on full thermodynamic venting process of liquid hydrogen in an on-orbit storage tank. *Int. J. Hydrogen Energy* **2020**, *45*, 27792–27805. [CrossRef]
42. Wan, C.; Zhu, S.; Shi, C.; Bao, S.; Zhi, X.; Qiu, L.; Wang, K. Numerical simulation on pressure evolution process of liquid hydrogen storage tank with active cryogenic cooling. *Int. J. Refrig.* **2023**, *150*, 47–58. [CrossRef]
43. Zhang, C.; Li, C.; Jia, W.; Pang, Y. Thermodynamic study on thermal insulation schemes for liquid helium storage tank. *Appl. Therm. Eng.* **2021**, *195*, 117185. [CrossRef]
44. Sarath, S.R.; Jayakumar, J.S. Thermal destratification of cryogenic liquid storage tanks by continuous bubbling of gases. *Int. J. Hydrogen Energy* **2022**, *47*, 34504–34532. [CrossRef]
45. Liu, Z.; Wang, L.; Jin, Y.; Li, Y. Development of thermal stratification in a rotating cryogenic liquid hydrogen tank. *Int. J. Hydrogen Energy* **2015**, *40*, 15067–15077. [CrossRef]
46. Xue, W.; Liu, Z.; Yang, Y. Study on the thermo-mechanical coupling performance of fluid sloshing in a liquefied natural gas storage tank. *Energy Sources Part A Recovery Util. Environ. Eff.* **2025**, *47*, 1–18. [CrossRef]
47. Sun, X.; Liu, Z.; Xue, W.; Yang, Y. Study on thermodynamic response in liquefied natural gas storage tanks under static pressurization and sloshing conditions. *Asia-Pac. J. Chem. Eng.* **2024**, *19*, e3044. [CrossRef]
48. Saleem, A.; Farooq, S.; Karimi, I.A.; Banerjee, R. A CFD simulation study of boiling mechanism and BOG generation in a full-scale LNG storage tank. *Comput. Chem. Eng.* **2018**, *115*, 112–120. [CrossRef]
49. Zhou, R.; Zhu, W.; Hu, Z.; Wang, S.; Xie, H.; Zhang, X. Simulations on effects of rated ullage pressure on the evaporation rate of liquid hydrogen tank. *Int. J. Heat Mass Transf.* **2019**, *134*, 842–851. [CrossRef]
50. Mer, S.; Thibault, J.-P.; Corre, C. Influence of non-condensable gases on thermodynamic control on-ground experiments using a substitute fluid. *J. Therm. Sci. Eng. Appl.* **2018**, *10*, 021006. [CrossRef]
51. Liu, Z.; Yin, X.; Liu, Y.; Li, Y.; Andersson, M. Thermodynamic performance in a liquid oxygen tank during active-pressurization under different gas injection temperatures. *Int. Commun. Heat Mass Transf.* **2023**, *140*, 106477. [CrossRef]
52. Liu, Z.; Pan, H.; Liu, Y.; Li, Y. Thermodynamic performance on the pressurized discharge process from a cryogenic fuel storage tank. *Int. J. Hydrogen Energy* **2022**, *47*, 12107–12118. [CrossRef]
53. Liu, Z.; Yang, Y.; Liu, Y.; Li, Y. Effect of gas injection mass flow rates on the thermal behavior in a cryogenic fuel storage tank. *Int. J. Hydrogen Energy* **2022**, *47*, 14703–14713. [CrossRef]
54. Liu, Z.; Feng, Y.; Lei, G.; Li, Y. Thermal physical process in a liquid oxygen tank under different sloshing excitations. *Int. Commun. Heat Mass Transf.* **2020**, *117*, 104771. [CrossRef]
55. Liu, Z.; Feng, Y.; Yan, J.; Li, Y.; Chen, L. Dynamic variation of interface shape in a liquid oxygen tank under a sinusoidal sloshing excitation. *Ocean Eng.* **2020**, *213*, 107637. [CrossRef]
56. Liu, Z.; Cai, H.; Feng, Y.; Liu, Y.; Li, Y. Thermodynamic characteristic in a cryogenic storage tank under an intermittent sloshing excitation. *Int. J. Hydrogen Energy* **2020**, *45*, 12082–12094. [CrossRef]
57. Liu, Z.; Feng, Y.; Cui, J.; Lei, G.; Li, Y. Effect of excitation types on sloshing dynamic characteristics in a cryogenic liquid oxygen tank. *J. Aerosp. Eng.* **2019**, *32*, 04019096. [CrossRef]
58. Liu, Z.; Cui, J.; Yan, J.; Zhou, G.; Li, Y. Effect of initial parameter on thermodynamic performance in a liquid oxygen tank with pressurized helium gas. *Sci. Technol. Built Environ.* **2019**, *26*, 426–436. [CrossRef]
59. Liu, Z.; Feng, Y.; Lei, G.; Li, Y. Hydrodynamic performance in a sloshing liquid oxygen tank under different initial liquid filling levels. *Aerosp. Sci. Technol.* **2019**, *85*, 544–555. [CrossRef]
60. Liu, Z.; Feng, Y.; Lei, G.; Li, Y. Sloshing hydrodynamic performance in cryogenic liquid oxygen tanks under different amplitudes. *Appl. Therm. Eng.* **2019**, *150*, 359–371. [CrossRef]
61. Liu, Z.; Li, Y. Thermal physical performance in liquid hydrogen tank under constant wall temperature. *Renew. Energy* **2019**, *130*, 601–612. [CrossRef]
62. Liu, Z.; Li, Y.; Jin, Y.; Li, C. Thermodynamic performance of pre-pressurization in a cryogenic tank. *Appl. Therm. Eng.* **2017**, *112*, 801–810. [CrossRef]
63. Liu, Z.; Li, Y.; Jin, Y. Pressurization performance and temperature stratification in cryogenic final stage propellant tank. *Appl. Therm. Eng.* **2016**, *106*, 211–220. [CrossRef]
64. Tiwari, P.; Maiti, D.K.; Maity, D. 3-D sloshing of liquid filled laminated composite cylindrical tank under external excitation. *Ocean Eng.* **2021**, *239*, 109788. [CrossRef]

65. Karimi, M.; Khorshidi, K.; Rezaeisaray, M.; Moutsanidis, G. Vibration of variable stiffness composite laminate and hybrid composite laminate plates coupled to sloshing fluid. *Compos. Struct.* **2022**, *292*, 115630. [CrossRef]
66. Pal, P.; Bhattacharyya, S.K. Slosh dynamics of liquid-filled composite containers—A two dimensional meshless local Petrov–Galerkin approach. *J. Fluids Struct.* **2013**, *39*, 60–75. [CrossRef]
67. Kim, D.-H.; Kim, S.; Kim, S.-W. Numerical analysis of drop impact-induced damage of a composite fuel tank assembly on a helicopter considering liquid sloshing. *Compos. Struct.* **2019**, *229*, 111438. [CrossRef]
68. Tiwari, P.; Maiti, D.K.; Maity, D. 3D sloshing frequency analysis of partially filled cylindrical laminated composite containers. *Int. J. Adv. Eng. Sci. Appl. Math.* **2024**, *16*, 117–132. [CrossRef]
69. Kormanikova, E.; Kotrasova, K. Multiscale modeling of liquid storage laminated composite cylindrical tank under seismic load. *Compos. Part B: Eng.* **2018**, *146*, 189–197. [CrossRef]
70. Moghaddasi, H.R.; Chakraborty, S.; Amabili, M. Nonlinear dynamics of simply supported, thin laminated circular cylindrical shells coupled to large-amplitude sloshing fluid. *Compos. Struct.* **2025**, *365*, 119148. [CrossRef]
71. Khorshid, K.; Farhadi, S. Free vibration analysis of a laminated composite rectangular plate in contact with a bounded fluid. *Compos. Struct.* **2013**, *104*, 176–186. [CrossRef]
72. Li, R.; Maschek, W.; Matzerath Boccaccini, C.; Vezzoni, B.; Flad, M.; Rineiski, A. Impact of the Bell–Plesset instability on centralized sloshing in pool geometry. *Int. J. Hydrogen Energy* **2016**, *41*, 7126–7131. [CrossRef]
73. Myrillas, K.; Planquart, P.; Buchlin, J.-M.; Schyns, M. Small scale experiments of sloshing considering the seismic safety of MYRRHA. *Int. J. Hydrogen Energy* **2016**, *41*, 7239–7251. [CrossRef]
74. Ryu M-r Yun, S.; Kim B-k Kang, D.; Kim, G.; Lee, H. Numerical analysis of sloshing effects in cryogenic liquefied-hydrogen storage tanks for trains under various vibration conditions. *Cryogenics* **2024**, *143*, 103961. [CrossRef]
75. Grotle, E.L.; Æsøy, V. Numerical simulations of sloshing and the thermodynamic response due to mixing. *Energies* **2017**, *10*, 1338. [CrossRef]
76. Duan, Z.; Zhu, Y.; Wang, C.; Yuan, Y.; Xue, H.; Tang, W. Numerical and theoretical prediction of the thermodynamic response in marine LNG fuel tanks under sloshing conditions. *Energy* **2023**, *270*, 126935. [CrossRef]
77. Zhu, Y.; Bu, Y.; Gao, W.; Xie, F.; Guo, W.; Li, Y. Numerical study on thermodynamic coupling characteristics of fluid sloshing in a liquid hydrogen tank for heavy-duty trucks. *Energies* **2023**, *16*, 1851. [CrossRef]
78. Ma, H.; Zhang, J. Numerical simulation study on the sloshing characteristics of cryogenic fuel in marine liquid hydrogen fuel tanks. In Proceedings of the 4th International Conference on Energy Engineering and Power Systems (EEPS), Hangzhou, China, 9–11 August 2024; IEEE: Piscataway, NJ, USA, 2024; pp. 74–78. [CrossRef]
79. Hauser, D.; Kassemi, M.; Kartuzova, O.; Baker, M.; Mishic, J. Mastering the cryogenic frontier: Predicting sloshing in cryogenic propellant tanks. In Proceedings of the 46th Annual AAS Guidance, Navigation and Control (GN&C) Conference, Littleton, CO, USA, 1–2 February 2024.
80. Sun, C.; Liu, L.; Wang, S.; Fan, X.; Li, Y.; Han, H. Visualization experimental and numerical study on multiphase flow characteristics of main cryogenic heat exchanger in offshore liquefied natural gas industry chain. *Cryogenics* **2022**, *124*, 103490. [CrossRef]
81. Simonini, A.; Peveroni, L.; Vetrano, M.R. Simultaneous interface position and bulk velocity measurements in cryogenic sloshing. *Aerosp. Sci. Technol.* **2019**, *90*, 452–462. [CrossRef]
82. Chen, H.; Xu, P.; Wan, Z.; Song, W.; Yang, G.; Wu, J. Analysis of convection and boil-off in multi-scale membrane LNG tanks under sloshing excitations. *Appl. Therm. Eng.* **2025**, *259*, 124863. [CrossRef]
83. Sreeraj, R.; Anbarasu, S. Numerical investigation of cryogenic liquid sloshing—A sigma transformation approach. In *Innovations in Energy, Power and Thermal Engineering*; Lecture Notes in Mechanical Engineering; Palanisamy, M., Natarajan, S.K., Jayaraj, S., Sivalingam, M., Eds.; Springer: Berlin/Heidelberg, Germany, 2022; pp. 229–239. [CrossRef]
84. Kang, W.; Gao, B.; Fan, X. Numerical study of the effect of sloshing on the properties of fluids in tanks of liquid hydrogen carriers. In Proceedings of the SPIE, 13172, Ninth International Symposium on Energy Science and Chemical Engineering (ISESCE 2024), 131720G, Nanjing, China, 22–24 March 2024. [CrossRef]
85. Zhang, H.; Chen, H.; Gao, X.; Pan, X.; Huang, Q.; Xie, J.; Chen, J. Numerical study on behaviors of the sloshing liquid oxygen tanks. *Energies* **2022**, *15*, 6457. [CrossRef]
86. Ma, B.; Yue, B.; Yan, S.; Lu, Y.; Upham, M.P.; Hao, B. Numerical and experimental study on the nonlinear liquid sloshing in Cassini tank. *J. Spacecr. Rocket.* **2025**, *62*, 466–476. [CrossRef]
87. Freeman, D. Sloshing analysis of an isothermal fluid in a cylindrical tank for cryogenic tank design using smoothed particle hydrodynamics. *Plymouth Stud. Sci.* **2024**, *17*, 3. [CrossRef]
88. Chen, H.; Wu, T.; Wan, Z.; Wang, H.; Xu, P.; Yang, G.; Wu, J. Numerical analysis of LNG rollover in large membrane tank under sloshing excitations. *Energy* **2025**, *315*, 134351. [CrossRef]
89. Grotle, E.L.; Æsøy, V. Dynamic modelling of the thermal response enhanced by sloshing in marine LNG fuel tanks. *Appl. Therm. Eng.* **2018**, *135*, 512–520. [CrossRef]

90. Liu, Z.; Feng, Y.; Lei, G.; Li, Y. Hydrodynamic performance on sloshing process in a liquid oxygen tank under intermittent excitation. *Cryogenics* **2019**, *98*, 92–101. [CrossRef]
91. Huang, C.; Wang, J.; Zhao, W.; Wan, D.C. Numerical simulation of liquid sloshing in a spherical tank by MPS method. *J. Hydrodyn.* **2024**, *36*, 232–240. [CrossRef]
92. Ryali, L.; Stautner, W.; Mariappan, D. Impact of internal baffle designs on liquid hydrogen sloshing in cryogenic aircraft fuel tanks. In *IOP Conference Series: Materials Science and Engineering*; IOP Publishing: Bristol, UK, 2024; Volume 1301, p. 012068. [CrossRef]
93. Li, L.; Shen, B.; Zhu, Z.; Ren, Q.; Zhang, J. Investigation of liquid sloshing characteristics in tanks using an OpenFOAM solver with arbitrary excitation. *AIP Adv.* **2024**, *14*, 115306. [CrossRef]
94. Li, C.; Zhao, Z.; Ding, J.; Liu, X.; Pu, X. Numerical study of thermodynamic and hydrodynamics in a type B LNG cargo tank during sloshing excitation. *Appl. Therm. Eng.* **2024**, *247*, 123048. [CrossRef]
95. Meng, L.; Sun, C.; Zhang, M.; Han, H.; Li, Y. Dynamic mesh simulation on the effect of sloshing on concurrent two-phase flow fields for two-dimensionally packed columns simulations. *Cryogenics* **2021**, *113*, 103231. [CrossRef]
96. Martinez, L.G.; Duret, B.; Reveillon, J.; Demoulin, F.X.; Jarry, A. Direct numerical simulation of sloshing and phase change in LH_2 tanks. In Proceedings of the Joint 10th European Conference for Aerospace Sciences (EUCASS) and 9th Conference of the Council of European Aerospace Societies (CEAS), Lausanne, Switzerland, 9–13 July 2023. [CrossRef]
97. Baker, M.C.; Hauser, D.M. Computational fluid dynamics simulation of methane slosh and drain experiments. In Proceedings of the AIAA SCITECH 2025 Forum, Orlando, FL, USA, 6–10 January 2025; American Institute of Aeronautics and Astronautics: Washington, DC, USA, 2025.
98. Han, H.; Du, Y.; Su, Z.; Liu, L.; Wang, J.; Li, Y. Shell-side heat transfer characteristics of floating liquefied natural gas spiral wound heat exchanger under sloshing conditions. *Appl. Therm. Eng.* **2023**, *232*, 121066. [CrossRef]
99. Rahbarimanesh, S.; Brinkerhoff, J.; Rahbarimanesh, A. Direct numerical simulation of a transitional, cryogenic cavitating mixing layer of liquefied natural gas behind a flat splitter plate using a homogeneous equilibrium mixture cavitation model. *Results Eng.* **2022**, *16*, 100781. [CrossRef]
100. Yang, C.; Niu, R.; Zhang, P. Numerical analyses of liquid slosh by finite volume and lattice Boltzmann methods. *Aerosp. Sci. Technol.* **2021**, *113*, 106681. [CrossRef]
101. Lv, H.; Chen, L.; Zhang, Z.; Chen, S.; Hou, Y. Numerical study on thermodynamic characteristics of large-scale liquid hydrogen tank with baffles under sloshing conditions. *Int. J. Hydrogen Energy* **2024**, *57*, 562–574. [CrossRef]
102. Lv, H.; Zhang, Z.; Chen, L.; Chen, S.; Yang, T.; Zhang, K.; Hou, Y. Study on thermohydrodynamic responses of liquid hydrogen in baffled tankers during braking process. *Int. J. Heat Fluid Flow* **2024**, *110*, 109612. [CrossRef]
103. Zuo, Z.Q.; Jiang, W.B.; Huang, Y.H. Effect of baffles on pressurization and thermal stratification in cryogenic tanks under micro-gravity. *Cryogenics* **2018**, *96*, 116–124. [CrossRef]
104. Liu, Z.; Li, C. Influence of slosh baffles on thermodynamic performance in liquid hydrogen tank. *J. Hazard. Mater.* **2018**, *346*, 253–262. [CrossRef]
105. Seban, A.; Srinivas, K.; Satyakumar, M.; Sarath Chandran Nair, S. Numerical slosh studies of multiple ring baffles in a semi-cryogenic fuel tank. In *Advances in Structural Integrity: Structural Integrity Over Multiple Length Scales*; Springer: Singapore, 2022; pp. 321–328.
106. Momin, S.; Kumar, P.; Salih, A. Numerical simulation of cryogenic fluid sloshing in propellant tank and influence of damping with ring baffles under forced excitations. In Proceedings of the 10th World Congress on Mechanical, Chemical, and Material Engineering (MCM'24), Barcelona, Spain, 22–24 August 2024. [CrossRef]
107. Gligor, D.; Peromingo, C.; Salgado Sánchez, P.; Porter, J.; Fernández, J.; Méndez, M.A. Sloshing mitigation in microgravity with moving baffles. *Acta Astronaut.* **2024**, *219*, 639–652. [CrossRef]
108. Bhavya, C.; Gomez, S.M.; Krishnakumar, R. Design and FE analysis of anti-slosh baffles for the fourth stage of PSLV. *Bonfring Int. J. Ind. Eng. Manag. Sci.* **2013**, *3*, 57. [CrossRef]
109. Liu, D.; Tang, W.; Wang, J.; Xue, H.; Wang, K. Hybrid RANS/LES simulation of sloshing flow in a rectangular tank with and without baffles. *Ships Offshore Struct.* **2017**, *12*, 1005–1015. [CrossRef]
110. Arif, U.G.M.; Loo, C.Y.; Kang, H.S.; Punurai, W.; Quen, L.K.; Lai, G.N.Y.; Chong, W.T. Suppression of hydrodynamic sloshing in liquefied natural gas tank with floating baffle: Experimental and numerical studies. In *IOP Conference Series: Earth and Environmental Science*; IOP Publishing: Bristol, UK, 2020; Volume 463, p. 012111. [CrossRef]
111. Abdullah, R.; Trimulyono, A.; Adietya, B.A. Numerical simulation of sloshing with floating baffles using smoothed particle hydrodynamics. In *IOP Conference Series: Earth and Environmental Science*; IOP Publishing: Bristol, UK, 2025; Volume 1461, p. 012007. [CrossRef]
112. Im, J.; Kwon, T.; Lee, S.; Kim, D.; Cho, H.; Won, W.; Gu, B. Unveiling the impact of internal structure on boil-off gas generation in moving liquid hydrogen (LH_2) transport trailer. *Renew. Sustain. Energy Rev.* **2025**, *216*, 115634. [CrossRef]
113. Prasad Varghese, A.; Hartwig, J.W.; Lieber, S.C.; Tafuni, A. Numerical design of a flow restrictor for tanked liquid nitrogen undergoing reduced-gravity flights. *Aerosp. Sci. Technol.* **2024**, *154*, 109539. [CrossRef]

114. Furuichi, Y.; Tagawa, T. Numerical study of the magnetic damping effect on the sloshing of liquid oxygen in a propellant tank. *Fluids* **2020**, *5*, 88. [CrossRef]
115. Rossetti, F.; Pirillo, L.; Cimini, M.; Bernardini, M.; Stella, F. Numerical investigation on the liquid sloshing damping inside a tank with a flexible anti-sloshing device. In Proceedings of the ICAS 2024 34th Congress of the International Council of the Aeronautical Sciences, Florence, Italy, 9–13 September 2024; ICAS: Firenze, Italy, 2024; pp. 9–13.
116. Wu, X.; He, R. Study on the influence of vertical baffles on liquid sloshing damping effect in vehicle fuel tank under resonance conditions. *Iran. J. Sci. Technol. Trans. Mech. Eng.* **2025**, *49*, 617–628. [CrossRef]
117. Chung, S.-M.; Jeon, G.-M.; Park, J.-C. Numerical approach to analyse fluid flow in a type C tank for liquefied hydrogen carrier (Part 1: Sloshing flow). *Int. J. Hydrogen Energy* **2022**, *47*, 5609–5626. [CrossRef]
118. Xue, M.-A.; Zheng, J.; Lin, P.; Yuan, X. Experimental study on vertical baffles of different configurations in suppressing sloshing pressure. *Ocean Eng.* **2017**, *136*, 178–189. [CrossRef]
119. Xue, M.-A.; Lin, P. Numerical study of ring baffle effects on reducing violent liquid sloshing. *Comput. Fluids* **2011**, *52*, 116–129. [CrossRef]
120. Xue, M.-A.; Jiang, Z.; Lin, P.; Zheng, J.; Yuan, X.; Qian, L. Sloshing dynamics in cylindrical tank with porous layer under harmonic and seismic excitations. *Ocean Eng.* **2021**, *235*, 109373. [CrossRef]
121. Zheng, J.; Xue, M.-A.; Dou, P.; He, Y. A review on liquid sloshing hydrodynamics. *J. Hydrodyn.* **2021**, *33*, 1089–1104. [CrossRef]
122. Mikishev, G.N.; Rabinovich, B.I. *Dynamics of Thin-Walled Structures with Compartments Containing Liquid*; Mashinostroenie Publ.: Moscow, Russia, 1971; pp. 541–559. 562p, Available online: https://library.bmstu.ru/Catalog/Details/134532 (accessed on 9 October 2025).
123. Jin, X.; Tao, Y.; Zhou, X.-C.; Yang, Y.-Z.; Luo, M.; Huang, J.-Z.; Fan, C.-Y. A novel fitness-based particle swarm optimization and radial basis function neural network for predicting liquid sloshing in tanks under seismic excitations. *Eng. Appl. Artif. Intell.* **2025**, *159 Pt A*, 111555. [CrossRef]
124. Liu, Q.-Q.; Wang, Z.-Y.; Qin, Y.-Y.; Xie, L.-M.; Chen, A.-Y.; Liu, J.; Jin, X. Intelligent prediction of seismically induced sloshing heights based on data augmentation. *Ocean. Eng.* **2025**, *339*, 122130. [CrossRef]
125. Ren, K.; Wu, G.X.; Li, Z.F. Natural modes of liquid sloshing in a cylindrical container with an elastic cover. *J. Sound Vib.* **2021**, *512*, 116390. [CrossRef]
126. Choudhary, N.; Bora, S.N.; Strelnikova, E. Study on liquid sloshing in an annular rigid circular cylindrical tank with damping device placed in liquid domain. *J. Vib. Eng. Technol.* **2021**, *9*, 1577–1589. [CrossRef]
127. Amabili, M.; Moghaddasi, H.R. Non-linear dynamics of cantilevered circular cylindrical shells with thickness stretch, containing quiescent fluid with small-amplitude sloshing. *J. Sound Vib.* **2024**, *571*, 118052. [CrossRef]
128. Jin, X.; Dai, C.; Tao, Y.; Chen, J.; Liu, M.M.; Zhang, C. Effects of seismic characteristics and baffle damping on liquid sloshing. *Phys. Fluids* **2024**, *36*, 013613. [CrossRef]
129. McNamara, K.P.; Awad, B.N.; Tait, M.J.; Love, J.S. Incompressible smoothed particle hydrodynamics model of a rectangular tuned liquid damper containing screens. *J. Fluids Struct.* **2021**, *103*, 103295. [CrossRef]
130. Jin, X.; Liu, M.; Zou, Y.; Luo, M.; Yang, F.; Wang, L. Numerical simulation of Faraday waves in a rectangular tank and damping mechanism of internal baffles. *J. Fluids Struct.* **2022**, *109*, 103503. [CrossRef]
131. Faltinsen, O.M.; Timokha, A.N. Natural sloshing frequencies and modes in a rectangular tank with a slat-type screen. *J. Sound Vib.* **2011**, *330*, 1490–1503. [CrossRef]
132. Zhao, C.; Wu, Y.; Yu, Y.; Haidn, O.J.; Hu, X. Liquid sloshing behaviours in an elastic tank and suppression effect of baffles. *arXiv* **2024**, arXiv:2409.16226. [CrossRef]
133. Luo, X.; Kareem, A.; Yu, L.; Yoo, S. A machine learning-based characterization framework for parametric representation of nonlinear sloshing. *arXiv* **2022**, arXiv:2201.11663. [CrossRef]
134. Jeon, G.-M.; Jeong, S.-M.; Park, J.-C. Experimental and numerical investigation of the influences of sloshing motion on the change in boil-off gas/boil-off rate in a cryogenic liquid tank. *Ocean Eng.* **2024**, *298*, 117173. [CrossRef]
135. Jin, X.; Tang, J.; Tang, X.; Mi, S.; Wu, J.; Liu, M.; Huang, Z. Effect of viscosity on sloshing in a rectangular tank with intermediate liquid depth. *Exp. Therm. Fluid Sci.* **2020**, *118*, 110148. [CrossRef]
136. Brodnick, J.; Sansone, M.; Yang, H. Gas Phase Effects on Slosh Dynamics. In Proceedings of the AIAA SCITECH 2025 Forum, Orlando, FL, USA, 6–10 January 2025; p. 0301. [CrossRef]
137. Kelly, M.; Fortune, M.; Borque, G.; Dooley, S. Machine learned compact kinetic models for methane combustion. *Combust. Flame* **2023**, *253*, 112755. [CrossRef]
138. Strahan, A.; Hernandez, H. Slosh baffle design and test for spherical liquid oxygen and liquid methane propellant tank for a lander. In Proceedings of the 47th AIAA/ASME/SAE/ASEE Joint Propulsion Conf. & Exhibit, San Diego, CA, USA, 31 July–3 August 2011; p. 5633. [CrossRef]
139. Yang, H.Q.; Williams, B. Validation of thermodynamics behaviors liquid propellant under sloshing and draining. In Proceedings of the AIAA SCITECH 2024 Forum, Orlando, FL, USA, 8–12 January 2024; p. 0548. [CrossRef]

140. Chegini, H.G.; Zarepour, G. Utilizing artificial neural network for load prediction caused by fluid sloshing in tanks. *Geofluids* **2021**, *1*, 3537542. [CrossRef]
141. Kim, K.J.; Kim, D. Prediction of sloshing pressure using image-based deep learning. *Ocean. Eng.* **2024**, *303*, 117718. [CrossRef]
142. Saghi, H.; Nezhad, M.R.S.; Saghi, R.; Sahneh, S.P. Comparison of artificial neural networks and genetic algorithms for predicting liquid sloshing parameters. *J. Mar. Sci. Appl.* **2024**, *23*, 292–301. [CrossRef]

Disclaimer/Publisher's Note: The statements, opinions and data contained in all publications are solely those of the individual author(s) and contributor(s) and not of MDPI and/or the editor(s). MDPI and/or the editor(s) disclaim responsibility for any injury to people or property resulting from any ideas, methods, instructions or products referred to in the content.